RIGA TECHNICAL UNIVERSITY

Ilijana Kovrlija

OCTACALCIUM PHOSPHATE BIOMATERIALS: FORMATION PROCESS, MODIFICATION AND APPLICATION

Summary of the Doctoral Thesis

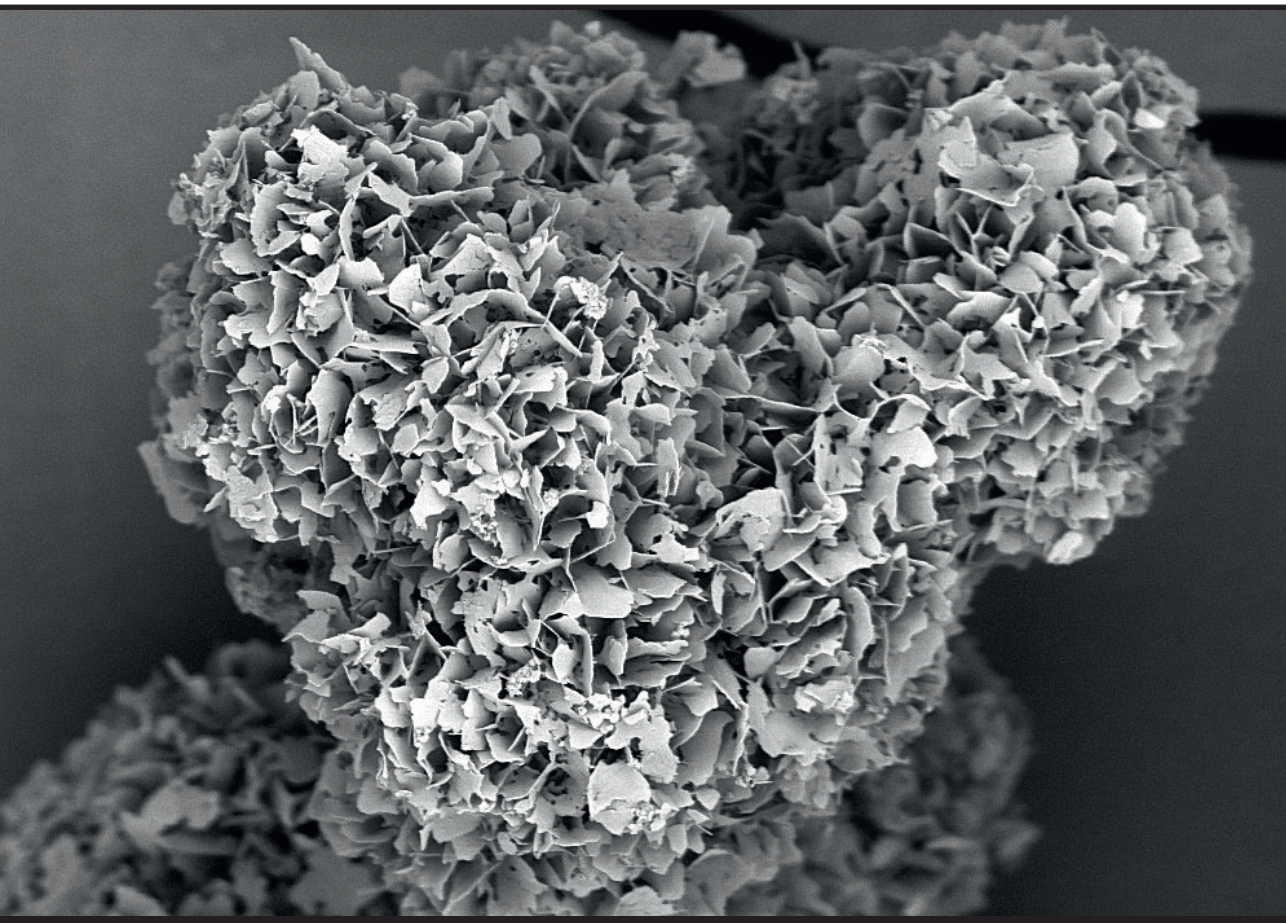

RTU Press
Riga 2024

RIGA TECHNICAL UNIVERSITY
Faculty of Natural Sciences and Technology
Institute of Biomaterials and Bioengineering

ILIJANA KOVRLIJA
Doctoral Student of the Study Programme "Chemistry, Materials Science and Engineering"

OCTACALCIUM PHOSPHATE BIOMATERIALS: FORMATION PROCESS, MODIFICATION AND APPLICATION

Summary of the Doctoral Thesis

Scientific supervisors
Professor Dr. sc. ing DAGNIJA LOČA
Professor Dr. sc. ing JĀNIS LOČS

RTU Press
Riga 2024

Kovrlija, I. Octacalcium Phosphate Biomaterials: Formation Process, Modification and Application. Summary of the Doctoral Thesis. Riga: RTU Press, 2024. 42 p.

Published in accordance with the decision of the Promotion Council "RTU P-02", June 03, 2024, Minutes No. 04030-9.2.2/4.

This work has been supported by the European Union's Horizon 2020 research and innovation programmes "Precision medicine for musculoskeletal regeneration, prosthetics, and active ageing" (No. 860462, PREMUROSA), "Baltic Biomaterials Centre of Excellence" (No. 857287, BBCE), and "Rising competitiveness of early-stage researchers and research management in Latvia" (No. 952347, RISEus2).

Cover picture by Ilijana Kovrlija

https://doi.org/10.7250/9789934371066

ISBN 978-9934-37-106-6 (pdf)

DOCTORAL THESIS PROPOSED TO RIGA TECHNICAL UNIVERSITY FOR THE PROMOTION TO THE SCIENTIFIC DEGREE OF DOCTOR OF SCIENCE

To be granted the scientific degree of Doctor of Science (Ph. D.), the present Doctoral Thesis has been submitted for the defense at the open meeting of the RTU Promotion Council on September 6, 2024, at 14:00, at the Faculty of Natural Sciences and Technology of Riga Technical University, 3 Paula Valdena Street, Room 272.

OFFICIAL REVIEWERS

Assistant Professor *Dr. sc. ing*. Agnese Brangule
Riga Stradins University, Latvia

Professor *Dr. chem*. Maris Turks
Riga Technical University, Latvia

Associate Professor *Dr*. Sabine van Rijt
Institute for Technology-Inspired Regenerative Medicine (MERLN), The Netherlands

DECLARATION OF ACADEMIC INTEGRITY

I hereby declare that the Doctoral Thesis submitted for review to Riga Technical University for the promotion to the scientific degree of Doctor of Science (Ph. D.) is my own. I confirm that this Doctoral Thesis has not been submitted to any other university for the promotion to a scientific degree.

Ilijana Kovrlija ……. (signature)
Date: 06.09.2024

The Doctoral Thesis has been written as a collection of articles. It consists of a summary in English and Latvian and five SCI publications. The publications have been written in English and have a total volume of 84 pages.

ANNOTATION

Within the present work, the synthesis methodology and upscaling of octacalcium phosphate (OCP) production from low-temperature α-tricalcium phosphate (α-TCP) have been optimized, and a comprehensive analysis profile of the obtained OCP has been established. To ultimately utilize the data from the physicochemical analysis, an *in silico* model capable of identifying the production stage of OCP has been designed. The developed OCP has been applied in two approaches: as a doxorubicin hydrochloride (DOX) drug delivery system for the treatment of osteosarcoma and as a protective coating against corrosion for titanium implants. The doxorubicin-octacalcium phosphate (DOX-OCP) drug delivery system was characterized, and the *in vitro* drug release and biological effects on MG63 (cancer cells) and MC3T3-E1 (normal cells) were studied. Sodium alginate/octacalcium phosphate (Alg/OCP) composite coatings were developed, and their electrochemical behavior on titanium alloys in inflammatory conditions was assessed.

The Doctoral Thesis has been written as a collection of articles. It consists of a summary in Latvian and English and five SCI publications. Each summary contains 15 figures and 1 table, followed by 5 appendices, totaling in 173 pages, including electronically available supplementary information.

TABLE OF CONTENTS

ACKNOWLEDGEMENT

Firstly, I would like to acknowledge the PREMUROSA, BBCE, and RISEus2 projects that financed my PhD and made it possible to visit all the incredible institutes, scientific conferences, and networking events.

There were many details and experiences that were important for me during the last four years, however I will mention only several of the most important ones.

First and foremost, I would like to thank my professors – Dagnija and Janis, who were there for me, not only as supervisors, but as friends and as a support system, whenever it was needed. I would like to thank you for millions of "fast questions", for numerous newly learned scientific facts, for a chance to show what I can achieve, for trusting me, for many parties and, the most important one, for showing me how to be a true mentor!

Also, I would like to thank my family – mom, dad, Danka, Sava, uncle, Dana and Vasilije. For your unconditional support to enroll in a PhD programme and for everything before and during my studies, without which none of this would be possible! To my best friends – Maja, Isidora, Maja and Daka – who were always there for me with their support and understanding! To Milica, for many hours of conversation on all the new things, cultures and work challenges! To Una and Kića, for the best and most important company that I was extremely lucky to have! To Aert, for all the support, love and laughter that made everything easier! And lastly, I would like to thank all of the people whom I met during this journey, who taught me many things and who I can now call my friends (you will recognize yourselves!)!

A special thank you goes to Jana and Līga, without whose help I would not have been able to submit my Thesis on time!

ZAHVALNICA

Postoje mnogi detalji i događaji koji su bili ključni tokom zadnjih četiri godine, ali ću da naglasim samo nekoliko najbitnijih.

Prije svega, htjela bih da se zahvalim mojim profesorima – Dagniji i Janisu, koji su bili uz mene, ne samo kao mentori, već kao i prijatelji i podrška kad god je to bilo potrebno. Htjela bih da Vam se zahvalim za milion „brzinskih pitanja", za mnogo novih naučenih činjenica, za šansu da pokažem šta mogu da postignem, za povjerenje, za mnoge žurke i kao najbitnije, za savršen primjer kako biti pravi mentor!!

Takođe, htjela bih da se zahvalim svojoj porodici – mami, tati, Danki, Savi, ujki, Dani i Vasiliju. Za vašu bezuslovnu podršku da upišem doktorat i za sve prije i tokom studija, bez čega ništa od ovoga ne bi bilo moguće! Mojim najboljim prijateljicama – Maji, Isidori, Maji i Daki, koje su uvijek bile tu za mene sa svojom podrškom i razumjevanjem! Milici, za mnoge sate razgovora oko novih stvari, kultura i poslovnih izazova! Uni i Kići, za najbolje i najvažnije društvo koje sam imala ogromnu sreću da ostvarim! Aertu, za svu podršku, ljubav i osmjehe koji su sve olakšali! I na kraju, željela bih da se zahvalim svim osobama koje sam upoznala na ovom putovanju, koje su me naučile mnogim stvarima i koje mogu sad da nazovem prijateljima (vi ćete se lako prepoznati!)!

Posebno se želim zahvaliti Jani i Ligi, bez čije pomoći ne bih mogla da predam tezu na vrijeme!

ABBREVIATIONS

ACP	amorphous calcium phosphate
Alg	sodium alginate
Alg/OCP	alginate/octacalcium phosphate
BET	Brunauer–Emmett–Teller method
CaP(s)	calcium phosphate(s)
CDHAp	calcium deficient hydroxyapatite
CPE	constant phase element
CPE_{dl}	interface between a substrate and a solution
DCPD/Brushite	dicalcium phosphate dihydrate
DDS(s)	drug delivery system(s)
DLC	drug loading capacity
DOX	doxorubicin hydrochloride
DOX-OCP	doxorubicin-loaded octacalcium phosphate
nDOX-OCP	n wt% of active substance (from the initial low temperature-α-tricalcium phosphate amount)
EIS	electrochemical impedance spectroscopy
Fer-1	ferrostatin-1
FTIR	Fourier transform infrared spectroscopy
HAp	hydroxyapatite
hBMSC	human bone mesenchymal stem cells
I	inflammatory medium
ICDD	International Centre for Diffraction Data
LT-α-TCP	low temperature-α-tricalcium phosphate
ML	Machine learning
N	normal medium
NMR	nuclear magnetic resonance
OCP	octacalcium phosphate
OS	osteosarcoma cells
PARP	poly (ADP-ribose) polymerase
PBS	phosphate buffered saline
PBT	polybutylene terephthalate
PCD	programmed cell death
PEGT	polyethylene glyco terephthalate
Rc	resistance
Rct	resistance to charge transfer
SEM	scanning electron microscopy
SI	severe inflammatory medium
SSA	specific surface area
TCP (α, β)	tricalcium phosphate (α, β)
TEM	transmission electron microscopy

TGA	thermogravimetric analysis
Ti Gr2	99.3 wt% titanium balance
Ti Gr23	Al 5.4 wt %, V 3.8 wt%, Fe 0.2 wt%, C 0.009 wt% of titanium balance
XRD	X-ray diffraction

GENERAL OVERVIEW OF THE THESIS

Introduction and Literature Review

Due to an increasing number of people having musculoskeletal diseases (322.75 million incident cases in 2019) [1], bone cancers (by 2040, global cancer cases will reach 26 million [2]) or incomplete regeneration of bones, it is detrimental to guide the research in the direction of finding the most effective solutions, which are able to help in the treatment of bone defects and bone tissue regeneration. Regenerative medicine's main endeavor is to mimic the properties of the native bone as closely as possible so the entire regeneration process can be faster and easier for the patients. Considering that using different drugs is also necessary to battle certain diseases, an additional goal is to minimize the aftermath of the systemic distribution that can have a lethal outcome. Nevertheless, irrespective of the end application, a suitable material needs to closely align to the golden standard: be biocompatible, biodegradable and exhibit osteoinductive properties (engagement and stimulation of cells to differentiate into preosteoblasts [3]).

Calcium phosphates (CaPs) are highly effective and reliable materials [4], biocompatible, osteoconductive, have the ability to incorporate different drugs/ions, and they are also the main constituents of bone's and teeth's inorganic part [5–8]. CaPs can be classified by their Ca/P molar ratio, solubility, crystallinity, particle size, morphology and specific surface area (SSA), but also based on their final form (nanoparticles, scaffolds, coatings, etc.). Hydroxyapatite (HAp, $Ca_{10}(PO_4)_6(OH)_2$), the most commonly used phase, is also naturally present in hard tissues (in non-stoichiometric form). Even though HAp is the most stable phase under physiological conditions, the disadvantage to using it could be slow resorption kinetics [9,10]. The second most often used CaP is tricalcium phosphate (TCP, $Ca_3(PO_4)_2$). The two polymorphs of TCP are α and β, and they are mostly used for bone regeneration [11], for example, α-TCP is extensively used in bone cements and other bone substitutes, as it has excellent biocompatibility and it showed positive results in *in vivo* [8]. Conversely, α-TCP has too high degradation rate when compared to the new bone growth rate [12,13]. Three out of all CaPs are presumed to be the precursors of bone apatite – amorphous calcium phosphate (ACP, $Ca_3(PO_4)_2 \cdot nH_2O$), dicalcium phosphate dihydrate (brushite or DCPD, $CaHPO_4 \cdot 2H_2O$), and octacalcium phosphate (OCP, $Ca_8(HPO_4)_2(PO_4)_4 \cdot 5H_2O$) [8,14]. ACP exhibits higher solubility and resorption rates, facilitated by lack of crystallinity, the presence of a hydrated layer, and the existence of defects, which ultimately contribute to the improved bioactivity [15,16]. DCPD has layers (sheets of CaO and PO_4^{3-}) that are parallel to the c-axis and are held together by hydrogen bonds from the water molecules within the structure [17,18]. DCPD forms in acidic aqueous solutions at pH 2–6, and one of the major DCPD's advantages is the strong inclination to transform to OCP or calcium deficient hydroxyapatite (CDHAp), which is why it is often used in self-setting CaP cements.

The third precursor, i.e., OCP, is the most similar one to HAp. The similarity lies in its structure – apatite layers being parallel to the (100) plane with hydrated layers in between [19,20]. This particular arrangement of apatite crystallographic planes (~ 1.1 nm thickness) and

a relatively empty hydrated layer (~ 0.8 nm thickness) [21], enables OCP to transform itself to the thermodynamically more stable phase, CDHAp, both *in vitro* and *in vivo* [21,22]. The presence of water molecules in the hydrated layer influences the level of the similarity of OCP structure to the one of HAp. Comparable conversion of OCP to apatite transpires in the process of bone formation [8]. Moreover, due to the presence of the hydrated layer, the incorporation of different ions and molecules is significantly more attainable [23]. From the biological point of view, the release of the HPO_4^{2-} ions from OCP [24] facilitates the stimulation of main bone cells (e.g., osteoblasts, osteocytes, osteoclasts [25]) and helps in enhancing macrophage migration to the implantation site [21]. Several studies showed that OCP can decrease the secretion of proinflammatory cytokines (necrosis factor-alpha and Interleukin-1), which show anti-inflammatory properties [26,27]. Also, multiple groups showed evidence of OCP's osteoinductivity – OCP-coated titanium [28] and OCP-coated polyethylene glyco-terephthalate/polybutylene terephthalate (PEGT/PBT) [29].

There are two main pathways for synthesizing OCP: the precipitation [20,30] and the hydrolysis [17,31]. The starting sources of calcium (Ca^{2+}) and phosphate (PO_4^{3-}) ions vary, and usually, in precipitation, they are combinations of calcium acetate, calcium carbonate, sodium acid phosphate and phosphoric acid, whereas in hydrolysis, the most common precursors are DCPD or α-TCP. Both processes are quite complex, and they depend on the intertwined effects of the pH, temperature, stir rate, ionic strength, etc. [23,32]. For example, if the temperature in the system is higher, the time until OCP materializes is shorter due to the more kinetically conducive conditions, which favor the formation of this phase. Alternatively, if the pH increases, it could lead to the precipitation of another phase (e.g., CDHAp). The aforementioned factors can also influence the size and morphology of the crystals (precipitation can result in thin elongated and lamellar particles, whereas hydrolysis can exhibit thin plate-like particles mixed with finer whisker-like particles) and the biological effect it will have [20,33]. Owing to this, the appropriate synthesis conditions must be chosen, depending on not only phase purity but also final morphology and the application of OCP.

To determine the CaP phase, its characteristic markings and morphology, a multi-technique characterization approach is necessary. To confirm the presence of a specific phase, X-ray diffraction (XRD), Fourier transform infrared spectroscopy (FTIR), Raman spectroscopy, scanning electron microscopy (SEM), nuclear magnetic resonance (NMR), thermogravimetric analysis (TGA), transmission electron microscopy (TEM), Brunauer–Emmett–Teller method (BET), Laser granulometry, etc. are being used. However, the downside of OCP (a very high similarity to CDHAp [23]) creates difficulty in claiming the phase purity quantitatively (overlap of XRD maxima with CDHAp can disrupt the Rietveld analysis). Other obstacles detected during the course of the literature review were relatively small yields of the obtained pure product (~ 100 mg – 2 g), a narrow region of pH (5.0–7.0 pH), temperatures favorable for the synthesis of OCP, and the inability to process it under high temperatures (> 80 °C) [23].

As the ongoing research progresses, innovative ways to employ OCP in regenerative medicine are being explored. OCP has been used as a bone cement [34] and as a composite scaffold with polymers (alginate, gelatin, collagen, PEGT, etc.) for the reconstruction of bone defects [35–37]. Also, as a coating on titanium alloy implants to enhance the biological

performance of the metal surfaces [29,38]. Considering the additional objective of regenerative medicine is to address systemic conditions like osteoporosis and minimize drug intake frequency and toxicity in cancer patients, the integration of bioactive ions and drugs into the CaPs has gained considerable popularity. When it comes to OCP, several ion substitutions (carbonate (CO_3^{2-}), magnesium (Mg^{2+}), zinc (Zn^{2+}), and strontium (Sr^{2+})) have been done to tune the bioactive effects [23]. Moreover, OCP has been used as a drug delivery system (DDS) to improve the biodistribution of therapeutics (bisphosphonates, ibuprofen, methotrexate) via local delivery pathways [23]. The conventional systemic drug delivery route operates through the circulatory system, potentially resulting in various side effects, systemic toxicity, and suboptimal delivery to the targeted site [39]. To mitigate these drawbacks, local agent delivery aims to reduce the burst release and to establish a tailored drug release profile, specific to the defect site. As malignant skeletal tumors (osteosarcoma (OS) standing out as a prominent representative), make up roughly 40 % of all bone tumors [2], some of the efforts on employing OCP as a carrier were directed to testing the effect of methotrexate-loaded OCP on OS cell lines [40], however research on OCP drug loading was mostly focused on bisphosphonates. Thus, it is crucial to devise a new DDS that effectively controls the localized administration and short/long-term effects of the anticancer drugs. It also enhances the applicability and mitigates the development of chemoresistance and dosage-dependent toxicity. It has been hypothesized that, if the drug loading is achieved *in situ* during the initial stages of OCP synthesis, it can lead to ultrahigh drug loading capacity (DLC) [41]. However, even though OCP has shown a high potential as a biologically active ion/molecule delivery system, there is scarce data on how the drug release mechanism from OCP works and how the process of drug/ion loading affects the formation of the OCP phase.

The rationale behind the proposed research

After a thorough review and bearing in mind the demonstrated importance of OCP, the Thesis focused on delivering systematic studies on OCP formation and utilization that were lacking in the literature, therefore filling the identified knowledge gap to some extent. Thus, within the Thesis, the optimization of the synthesis methodology and scale-up method of OCP synthesis was elaborated, anticancer drug-loaded OCP delivery systems were developed, and OCP applicability in composite coatings was tested. The comprehensive strategy of the PhD research is shown in Fig. 1.

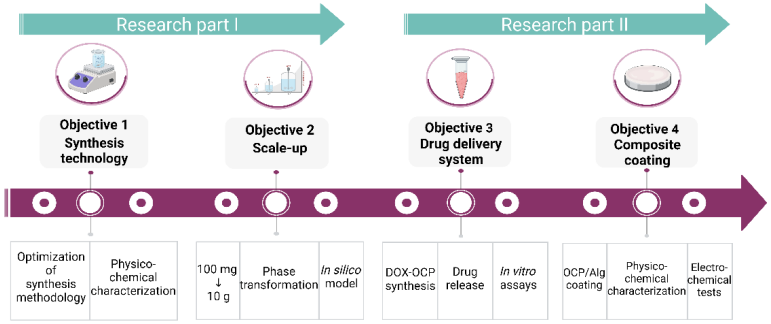

Fig. 1. PhD project roadmap. OCP – octacalcium phosphate; Alg – alginate; DOX – doxorubicin; DOX-OCP – doxorubicin loaded octacalcium phosphate.

Aim and Objectives

The aim of the Thesis was to optimize the synthesis technology to obtain a stable OCP with high phase purity and to explore its application as a drug delivery vehicle as well as a protective composite coating. To fulfil the aim, the following objectives were set:

1. To optimize the synthesis methodology of OCP via the hydrolysis of low-temperature α-tricalcium phosphate (LT-α-TCP) and study the physicochemical properties of the obtained OCP.
2. To optimize the scale-up of the synthesis technology, determine the formation pathway of OCP, and develop an *in silico* model for the determination of the OCP synthesis termination based on the XRD and FTIR results.
3. To develop a drug delivery system for cancer treatment by combining OCP with an anti-neoplastic agent – doxorubicin hydrochloride (DOX-OCP).
4. To develop the OCP-embedded hydrogel coatings for metallic implants able to enhance corrosion resistance.

Thesis to Defend

1. Hundredfold upscaling of OCP synthesis via the hydrolysis of LT-α-TCP at room temperature does not affect the physicochemical properties of the final product (phase composition, molecular structure and morphology).
2. Doxorubicin can be incorporated into the octacalcium phosphate particles up to 10 wt% of the initial OCP precursor amount, while higher amounts of doxorubicin inhibit the OCP phase formation. The as-synthesized product can serve as a prolonged-release anticancer drug delivery system.
3. If used in coatings for 3D printed Tibased metallic implants, OCP affects electrical charge transfer resistance at the substrate and coating interface.

Scientific Novelty

The scientific novelty was recognized in the following aspects:

1. By following the phase transformations from LT-α-TCP to OCP, it was established and described through chemical equations that the progressive shift from LT-α-TCP phase to the OCP phase transpired through DCPD as an intermediary point.
2. Maximum loading of doxorubicin hydrochloride during the *in situ* synthesis of OCP was 10 wt% (of the initial LT-α-TCP amount), whereas everything above inhibited the OCP formation. Furthermore, doxorubicin-loaded OCP caused apoptosis as the main cell death pathway.

Practical Significance

OCP's simple and straightforward synthesis methodology was optimized by choosing LT-α-TCP as a single precursor that required less energy consumption to produce, which aligned with the set goals of the European Green Deal. The synthesis methodology was further utilized to obtain high yields of OCP, which could be used on an industrial scale. The applicability of as-synthesized OCP is twofold:

1) in the development of a novel DDS for the local treatment of osteosarcoma, and
2) in the development of OCP-embedded hydrogel coatings for the enhancement of corrosion resistance of 3D-printed titanium alloys.

Publications and Approbation of the Thesis

The results of the Thesis were published in five SCI scientific publications.

1. **Kovrlija I**., Locs, J., Loca, D. Octacalcium phosphate: Innovative vehicle for the local biologically active substance delivery in bone regeneration, *Acta Biomaterialia*, 135, 2021, pp. 27–47. doi: 10.1016/j.actbio.2021.08.021 (Scopus, Open Access, IF 9.4, Q1, CiteScore 16.8).
    - Kovrlija, I. contributed to the publication by writing the original draft, reviewing and editing, and visualization (in total 85/100 %).
2. **Kovrlija, I.,** Menshikh, K., Marsan, O., Rey, C., Combes, C., Locs, J., Loca, D. Exploring the Formation Kinetics of Octacalcium Phosphate from Alpha-Tricalcium Phosphate: Synthesis Scale-Up, Determination of Transient Phases, Their Morphology and Biocompatibility, *Biomolecules*, 13, 2023, 462. doi:10.3390/biom13030462 (Scopus, Open Access, IF 4.8, Q1, CiteScore 9.4).
    - Kovrlija, I. contributed to the publication by writing the original draft, reviewing and editing, conceptualization, visualization, formal analysis, and investigation (in total 80/100 %).
3. Nascimben, M., **Kovrlija, I.,** Locs, J., Loca, D., Rimondini, L. Fusion and classification algorithm of octacalcium phosphate production based on XRD and FTIR data, *Scientific Reports*, 14:1489, 2024, 1–11. doi: 10.1038/s41598-024-51795-0 (Scopus, Open Access, IF 3.8, Q1, CiteScore 6.9).
    - Kovrlija, I. contributed to the publication through laboratory experiments, data collection and organization, results discussion, manuscript draft writing, manuscript editing and revision (in total 50/100 %).
4. **Kovrlija, I**., Pańczyszyn E., Demir, O., Laizane, M., Corazzari, M., Locs, J., Loca, D. Doxorubicin-loaded octacalcium phosphate particles as controlled release drug delivery systems: physico-chemical characterization, in vitro drug release and evaluation of cell death pathway, *International Journal of Pharmaceutics*, 653, 2024, 123932. doi: 10.1016/j.ijpharm.2024.123932 (Scopus, Open Access, IF 5.3, Q1, CiteScore 10.7).
    - Kovrlija, I. contributed to the publication through writing the original draft, reviewing and editing, conceptualization, visualization, formal analysis, and investigation (in total 75/100 %).
5. Bordbar Khiabani, A., **Kovrlija, I**., Locs, J., Loca, D., Gasik, M. Octacalcium Phosphate-Laden Hydrogels on 3D-Printed Titanium Biomaterials Improve Corrosion Resistance in Simulated Biological Media, *International Journal of Molecular Sciences*, 2023, 24, 13135. doi: 10.3390/ijms241713135 (Scopus, Open Access, IF 4.9, Q1, CiteScore 8.1).
    - Kovrlija I. contributed to the publication throughg writing – the original draft preparation, visualization, formal analysis, and investigation (in total 50/100 %).

The results of the Thesis were presented at nine scientific conferences.

1. **Kovrlija I**., Nascimben M., Bordbar-Khiabani A., Menshikh K., Gasik M., Combes C., Rimondini L., Locs J., Loca D. Tailoring the production technology and utilization of octacalcium phosphate for precise patient-centred applications in musculoskeletal field. *12th World Biomaterials Congress*, 26.-31. May 2024, Daegu, South Korea; (I.K. poster presentation).
2. **Kovrlija, I**., Demir, O., Laizane, M., Locs, J., Loca, D. Novel drug delivery vehicle: doxorubicin-loaded octacalcium phosphate. *33rd Annual Conference of the European Society of Biomaterials*, 04–08 September 2023, Davos, Switzerland. (I. K. – poster presentation).
3. **Kovrlija, I**., Menshikh, K., Demir, O., Locs, J., Loca, D., Octacalcium phosphate: journey of creating a unique drug delivery vehicle. *The XVIIIth Conference of the European Ceramic Society*, 02–06 July 2023, Lyon, France. (I. K. —student speech contest).
4. **Kovrlija, I**., Menshikh, K., Marsan, O., Rey, C., Combes, C., Locs, J., Loca, D. Scale-Up of Octacalcium Phosphate via Hydrolysis Route: Effect on Physico-Chemical Characteristics and In-Vitro Cytocompatibility with Bone Marrow-Derived Mesenchymal Stem Cells. *Tissue Engineering and Regenerative Medicine International Society European Chapter Meeting*, 28–31 March 2023, Manchester, UK. (I. K. – oral presentation).
5. **Kovrlija, I**., Menshikh, K., Marsan, O., Rey, C., Combes, C., Locs, J., Loca, D. Phase transformation from α-tricalcium phosphate to octacalcium phosphate via hydrolysis route. *Scandinavian Society for Biomaterials 16th annual meeting*, 21–14 March 2023, Roros, Norway. (I. K. – poster presentation).
6. **Kovrlija, I.,** Barbut, C., Locs, J., Loca, D. Incorporation and effect of lidocaine hydrochloride on octacalcium phosphate. *32nd Annual Conference of the European Society of Biomaterials*, 04–08 September 2022, Bordeaux, France. (I. K. – poster presentation).
7. **Kovrlija, I**., Locs, J., Loca, D. Unravelling the Behaviour of Octacalcium Phosphate in Various Model Solutions. *Scandinavian Society for Biomaterials 15th annual meeting*, 13–15 June 2022, Jurmala, Latvia. (I. K. – poster presentation).
8. **Kovrlija, I.,** Barbut, C., Locs, J., Loca, D. Effects of the synthesis conditions on the hydrolysis of α-tricalcium phosphate to octacalcium phosphate. *31st Annual Conference of the European Society for Biomaterials*, 2021 (online). (I. K. – poster presentation).
9. **Kovrlija, I**., Locs, J., Loca, D. Octacalcium phosphate: a contemporary drug delivery system for local biologically active substances – a review. *Scandinavian Society for Biomaterials 14th Annual Meeting*, 2021 (online). (I. K. – poster presentation).

The results of the PhD Thesis were presented at other scientific events.

1. Locs, J., **Kovrlija, I**., Choudhary, R., Loca, D. Roadmap from upscaling and rapid synthesis towards first-ever consolidation of OCP. *33rd Conference and annual meeting of the International Society for Ceramics in Medicine*, 17–20 October 2023, Solothurn, Switzerland. (J.L. invited talk).
2. Bordbar Khiabani, A., **Kovrlija, I.,** Locs, J., Loca, D., Gasik, M. Octacalcium Phosphate Embedded Hydrogels on 3D Printed Titanium Improve the Corrosion Performance in Simulated Biological Media. *31st Annual Meeting of European*

Orthopaedic Research Society, 27–29 September 2023, Porto, Portugal. (A. B. K. – oral presentation).

3. Loca, D., **Kovrlija, I.,** Pylostomou, A., Locs, J. Can Octacalcium Phosphate Be Used as a Doxorubicin Delivery Platform? *Tissue Engineering and Regenerative Medicine International Society – Americas Chapter Annual Meeting*, 11–14 April 2023, Boston, USA. (D. L. – poster presentation).
4. Menshikh, K., **Kovrlija, I.,** Miola, M., Cochis, A., Rimondini, L. Synthetic pre-vascularized porous scaffold as an engineered environment for the in vitro osteosarcoma model. *Tissue Engineering and Regenerative Medicine International Society European Chapter Meeting*, 28 June – 1 July 2022, Krakow, Poland. (K. M. – poster presentation).
5. Menshikh, K., **Kovrlija, I**., Miola, M., Cochis, A., Rimondini, L. Freeze-dried Composition of Alginate and Bioglass as an Engineered Environment for the Osteosarcoma Model. *Scandinavian Society for Biomaterials 15th annual meeting*, 13–15 June 2022, Jurmala, Latvia. (K. M. – poster presentation).
6. **Kovrlija, I**., Locs, J., Loca, D. Octacalcium phosphate: synthesis, characterization and functionalization. *4th Premurosa Summer School*, 15–19 May 2024, Riga, Latvia. (I. K. – oral presentation).
7. **Kovrlija, I**., Locs, J., Loca, D. Unravelling the Behaviour of Octacalcium Phosphate in Various Model Solutions. *3rd Premurosa Summer School*, 20–24 June 2023, Belgrade, Serbia. (I. K. – poster presentation).
8. **Kovrlija, I.,** Locs, J., Loca, D. Smart personalized degradable biomaterials for bone tissue regeneration. *2nd Premurosa Summer School*, 19–24 October 2022, Porto, Portugal. (I. K. – oral presentation).
9. **Kovrlija, I**., Loca, D. Octacalcium phosphates: promising instruments for local drug delivery in bone regeneration. Baltic Biomaterials Centre of Excellence Summer School on "Scientific writing", 23–27 November 2020, online. (I. K. – oral presentation).

Other scientific publications published during the development of the Thesis.

1. **Kovrlija I**., K. Menshikh, H. Abreu, A. Cochis, L. Rimondini, O. Marsan, C. Rey, C. Combes, J. Locs, D. Loca, Challenging Applicability of ISO 10993-5 for Calcium Phosphate Biomaterials Evaluation: Towards More Accurate In Vitro Cytotoxicity Assessment, *Biomaterials Advances*, 160, 213866, 2024. doi: 10.1016/j.bioadv.2024.213866 (Scopus, Open Access).
2. Aunina, K., Ramata-Stunda, A., **Kovrlija, I**., Tracuma, E., Merijs-Meri, R., Nikolajeva, V., Loca, D. Exploring the Interplay of Antimicrobial Properties and Cellular Response in Physically Crosslinked Hyaluronic Acid/ε-Polylysine Hydrogels, *Polymers*, 15(8): 1915, 2023. doi:10.3390/polym15081915 (Scopus, Open Access).
3. Mosina, M., **Kovrlija, I**., Stipniece, L., Locs, J. Gallium containing calcium phosphates: Potential antibacterial agents or fictitious truth, *Acta Biomaterialia*, 150, 48–57, 2022. doi: 10.1016/j.actbio.2022.07.063 (Scopus, Open Access).
4. **Kovrlija, I**., Locs, J., Loca, D. Incorporation of Barium Ions into Biomaterials: Dangerous Liaison or Potential Revolution? *Materials*, 14(19), 2021, p. 5772. doi: 10.3390/ma14195772 (Scopus, Open Access).

MAIN RESULTS OF THE THESIS

Optimization of OCP synthesis methodology

Despite the fact that the potential of OCP to stimulate bone regeneration is reported to be higher than that of HAp [3,42,43], a moderately narrow window of opportunity to obtain it and the complexity of synthesis hinders the scientific community, as well as industry, from proactive involvement [23,32]. Both key routes to obtain OCP have their advantages and disadvantages, and the main pros and cons are highlighted in Table 1.

Table 1

Advantages and Disadvantages of Precipitation and Hydrolysis Routes for OCP Synthesis [31, 44-47].

Precipitation		**Hydrolysis**	
Pros	**Cons**	**Pros**	**Cons**
Faster reaction	Minimum two precursors	Only one precursor	Slower reaction
Higher yields	Dose rate regulation	No dose rate	Yield is limited to the initial precursor amount
/	Higher temperatures (60 °C–80 °C)	Lower temperatures (25 °C–60 °C)	/
/	Washing of the precipitate needed	No washing step	/
/	pH regulation always needed	pH regulation could be avoided	/

Hydrolysis of low-temperature α-TCP to OCP

After considering the pros and cons of the synthesis pathways, the hydrolysis route aligned more with the proposed objectives of the PhD Thesis. According to the literature, both DCPD and α-TCP have been used as precursors in hydrolysis. However, DCPD has higher solubility than α-TCP, it can be more easily affected by carbon dioxide from the atmosphere, and in lower temperatures (< 30 °C), it takes months to transform to OCP [21]. Thus, α-TCP has been chosen as the sole precursor in OCP synthesis.

Traditionally, the synthesis of α-TCP involves heating the materials that contain calcium and phosphate, such as β-TCP, to temperatures of 1300 °C or higher for an extended duration (~ 2–3 h). This conventionally synthesized α-TCP manifests as a coarse powder necessitating subsequent milling, which yields particles with a wide size distribution and generates an

amorphous phase [44]. To avoid it and to use a more energy-efficient way, low-temperature α-TCP (LT-α-TCP) was made from ACP with high SSA (> 70 m^2/g) (precipitation from diammonium phosphate solution and calcium nitrate tetrahydrate solution) that was heat treated at 650 °C (Fig. 2) [44].

The following OCP synthesis was performed in the acidic media (0.0016 M orthophosphoric acid (H_3PO_4) from the aforementioned LT-α-TCP, with unremitting stirring, at room temperature (22 °C) [45]. The samples were dried at 37 °C (overnight), and, to evaluate whether the obtained OCP was pure, the products were subjected to multiple analysis techniques (see Fig. 2).

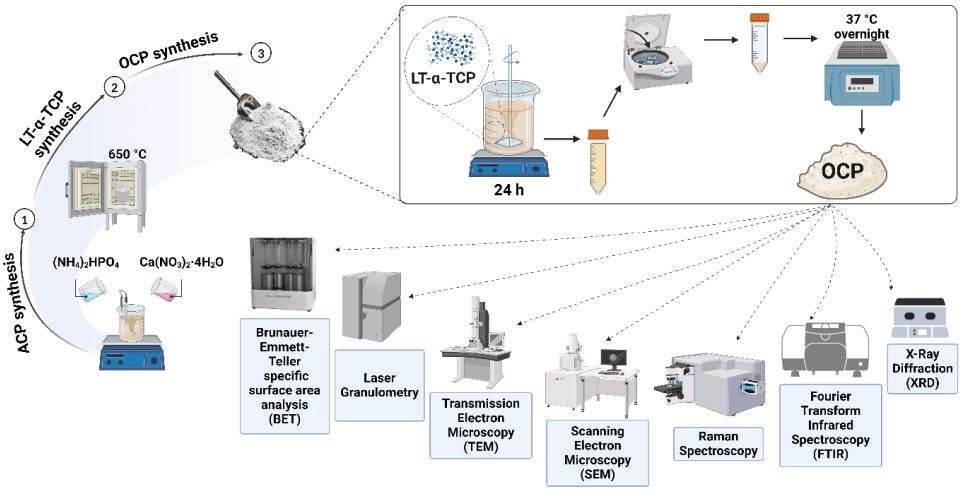

Fig. 2. General scheme of OCP synthesis methodology and overview of the used characterization methods in determining the OCP phase.

The as-synthesized sample (marked with OCP1) has been analyzed with a set of preselected characterization methods able to deliver the data on different levels. Phase compositions were studied with the X-ray diffraction technique (XRD, PANalytical Aeris diffractometer, The Netherlands), and the crystalline phase identification was done by using the PDF-2 database from the International Centre for Diffraction Data (ICDD). To get the information on the phases at the molecular level, Fourier transform infrared spectroscopy (FTIR, Nicolet iS 50, Thermo Scientific, USA) and Raman spectroscopy (LabRAM HR 800 microscope, Horiba Jobin Yvon, Japan) have been used as the chosen techniques. The morphology of the powders was characterized with scanning electron microscopy (SEM, Tescan Mira\LMU, Tescan, Czech Republic) and transmission electron microscopy (TEM, Tecnai F20, FEI). Particle size distribution was determined using laser granulometry (Malvern Mastersizer 3000), whereas specific surface area was measured using Brunnauer–Emmet–Teller method (BET, QUADRASORB SI and Quadra Win).

The XRD pattern of OCP is very specific. The characteristic low angle (100) maxima at 4.72 2θ degrees and a peak doublet at 9.44 (200) 2θ degrees and 9.77 (010) 2θ degrees (Fig 3 A), were shown in the obtained OCP1 [46]. Even though these markings make OCP easy to

recognize among other CaPs, the region of 25–35 2θ degrees is known to overlap with the XRD maxima of HAp (Fig. 3 A), due to the close relationship of OCP and HAp structures [46–48]. However, the lack of HAp maxima at 10.8 2θ degrees is one indicator of no or minimal HAp presence. Another important part to observe is the aforementioned doublet at 9.4 and 9.7 2θ degrees because the most intense OCP peak (4.7) is superimposed to the X-ray diffusion background, hence not easily accessible and affected by the plate-like morphology that causes preferential orientations. The influence of the background can later interfere with Rietveld's calculations used to determine the quantity of the specific phase.

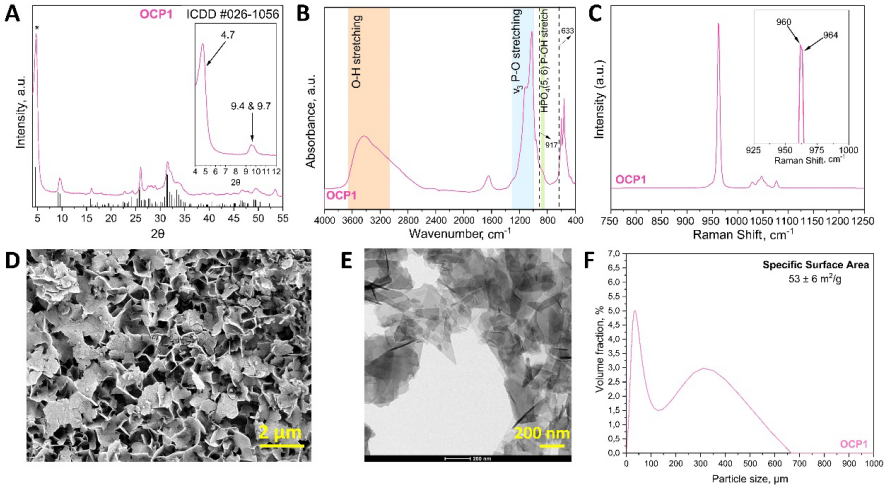

Fig. 3. A set of analyses confirming the obtained OCP purity: A – XRD diffractogram; B – FTIR spectra; C – Raman spectra; D – SEM micrograph; E – TEM micrograph; F – Particle size distribution and SSA (* – the XRD peak at 4.7 2θ degrees).

Another distinctive feature of OCP's unit cell is two HPO_4^{2-} crystallographic sites, labeled $HPO_4(5)$ and $HPO_4(6)$; their P–(OH) stretch and OH in-plane bend cannot be distinguished via the XRD method. The $HPO_4(5)$ group is situated in the hydrated layer, and the $HPO_4(6)$ group is located at the junction of the apatite and hydrated layers; however, they are different ($HPO_4(6)$ has a shorter and stronger intermolecular hydrogen bond than that of $HPO_4(5)$) [49]. HPO_4 groups are not found in HAp, and their presence can further discriminate between these two phases. Therefore, FTIR and Raman spectroscopy were used to examine the samples' molecular structure and help to confirm the purity of the OCP phase (Fig. 3 B and C) [49]. Specific OCP absorbance bands that differentiate it from other CaPs were highlighted in OCP1 spectra – HPO_4^{2-} bending and O–H stretching modes (Fig. 3 B, orange and green shading). The most significant HPO_4 absorbance bands assigned to OCP are: 1295 cm^{-1} (OH in-plane deformation mode) and 917 cm^{-1} (P(6)–(OH) stretch of a strongly hydrogen-bonded HPO_4^{2-} ion), also the v3 stretching mode of PO_4^{3-} and HPO_4^{2-}, at 1077 cm^{-1}, 1093 cm^{-1}, and 1121 cm^{-1}. The absence of a detectible 3572 cm^{-1} OH^- band for HAp is one of the pointers of a pure OCP formation (or at least with a negligible HAp presence, shown in [45]). OH^- absorbance band at 633 cm^{-1}, usually assigned to the OH^- libration movement in HAp, was found as a shoulder in

OCP (627 cm^{-1}); however, according to Fowler et al. [49], it also represents a libration movement of the $H_2O(4)$ water molecule of OCP. In Raman spectra, the most intense bands are located between 900–1000 cm^{-1}, corresponding to the ν_3 triple-degenerate asymmetric P–O stretching mode and partly to the ν_1 symmetric P–O stretching vibration. A specific band for OCP is located at 958 cm^{-1} (Fig. 3 C, most intense peak) [49]. However, the large mass may also be associated with the convolution of several crystalline phases composed of the main band at 960 cm^{-1} and the shoulder at 964 cm^{-1}, associated with ν_1 PO_4 of OCP, and it could indicate a low crystallized OCP phase.

OCP crystals exhibit plate-like morphology, and the sizes of the crystals depend on the synthesis route. The formation of the particular OCP crystals is thought to be connected to the Hartman–Perdok theory of periodic bond chains, which says that a constant path of strong bonds within the crystal structure has a portion of the lattice that is cut by a certain face (hkl) [47]. For OCP, the plates grow in the [001] direction, with the largest face (100), and these interconnections lead to the formation of spherical aggregates that resemble sand roses. SEM analysis (Fig. 3 D) showed the surface morphology of OCP1, which resembled small, loosely aggregated plate-like particles (2–5 μm in size, thickness in nm range), interconnected in a rose shape. Small plate-like crystals of different sizes were seen when the OCP's inner structure was analyzed with TEM (Fig. 3 E) (50–300 nm approximately). It was also noticed that crystals were overlapping and entwining, which led them to form agglomerates of different sizes that were seen in SEM. BET measurements showed that OCP1 had a large SSA of 53 ± 6 m^2/g. The high value of SSA may suggest higher physicochemical and biological reactivity of the material, which could have a very strong effect on the cells. The evolution of the particle size distribution (a bimodal curve, Fig. 3 F) showed that the smallest primary particle size was in the array of 5–25 μm, totaling in ~ 5 % volume. The occurrence of the secondary distribution in the range of 150–500 μm indicated that the particles were unevenly agglomerated.

The first objective of the research was successfully achieved, and it demonstrated the feasibility of obtaining pure OCP powder from LT-α-TCP. However, the yield of the product was ~ 100 mg per batch, which was not sufficient for potential application and subsequent *in vitro/in vivo* studies. Consequently, an endeavor to augment the product's yield was initiated.

OCP synthesis scale-up, phase formation kinetics and *in silico* model of the synthesis progression from LT-α-TCP to OCP

After obtaining pure OCP from LT-α-TCP (at room temperature in 24 h, OCP1), the next step was to optimize the settings and try to achieve a higher product yield. The synthesis methodology of LT-α-TCP hydrolysis was scaled up a hundredfold (100 mg → 1g → 10 g). During the process of scale-up optimization, two additional aspects were followed – phase formation kinetics from LT-α-TCP to OCP and the development of an *in silico* model for tracking the stage of the OCP synthesis.

OCP synthesis scale-up

The acquired data have shown that with a constant liquid-to-solid ratio of the precursors, the time of the OCP synthesis has increased with the amount of the initial LT-α-TCP used. In the tenfold scale-up, the OCP phase was achieved after 72 h (OCP2, 1 g), and in the hundredfold scale-up, OCP was obtained after 180 h (OCP3, 10 g).

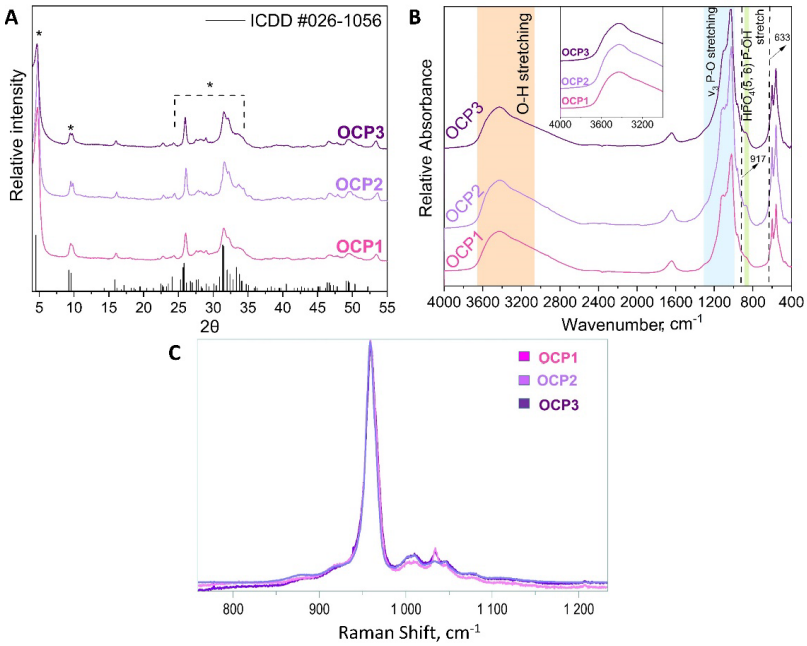

Fig. 4. Final OCP phases obtained in three levels of scale-up. A –XRD pattern; * marks the main maxima mentioned in the text, and the reference simulated pattern (ICDD entry #026-1056) corresponds to the main maxima of the OCP triclinic phase; B – FTIR spectra; C – Raman spectra.

Characteristic XRD peaks of OCP have been detected – 4.7 degrees and a doublet at 9.4 and 9.7 2θ degrees (Fig. 4 A) [23,50]. Same as in the original synthesis level (OCP1, 100 mg), the pattern in the region of 25–35 2θ degrees was not very well resolved [20]. FTIR ν_3P–O stretching mode at 1300–1000 cm^{-1}, for the OCP2 and OCP3 (Fig. 4 B), clearly showed the

strongest lines expected for the OCP phase, and in Raman, the ν_1P–O stretching mode was accentuated (Fig. 4 C). The assignment of the most specific bands of OCP was discussed in the previous section. To observe the possible variances of composition within a single sample, micro and macro spots in Raman were recorded and discussed within the manuscript [45]. The obtained results suggested that the formation and/or dissolution of the phases were closely linked to the size of the starting powder's grains (or aggregates).

According to the laser granulometry, both OCP2 and OCP3 had similar particle sizes as OCP1, whereas their specific surface area was slightly higher than that of OCP1, 66 ± 5 m^2/g and 63 ± 8 m^2/g, respectively.

OCP phase formation kinetics

A detailed progression of the OCP phase formation has been followed during the synthesis of OCP3 (10 g) as a function of time. The total duration of the synthesis was 180 h, and the pH was monitored throughout the entire time. Throughout the synthesis monitoring, the focus was placed on important XRD maxima of all present phases and the variations in the reaction media pH. XRD patterns were used to visualize the gradual evolution of the crystalline phase from LT-α-TCP, as an initial phase, towards the combination of LT-α-TCP, DCPD, and OCP, and ending with the pure OCP phase (Fig. 5) [51,52]. The characteristic maxima that were highlighted are maxima at 4.7, 9.4 and 9.7 2θ degrees (belonging to OCP triclinic structure), 11.7, 20.9 and 29.2 2θ degrees (belonging to DCPD monoclinic structure) and 12.1, 22.1 and 22.9 2θ degrees (belonging to α-TCP monoclinic structure).

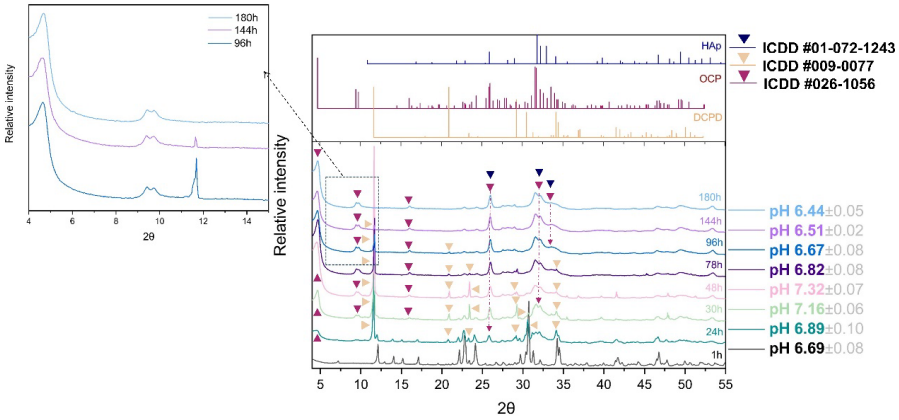

Fig. 5. Synthesis of OCP3: XRD patterns showing the transition from LT-α-TCP, via DCPD to OCP phase, supplemented by the change in pH. The reference simulated patterns (ICDDs) correspond to the main maxima of the HAp, OCP, and DCPD [45].

The variations in the pH helped to discern the underlying chemical background (through chemical equations) of the phase changes, as the release of ions (e.g. OH^-, H^+) directly influences the solution pH. The general chemical equation displaying the hydrolysis of LT-α-TCP to OCP is the following: $3Ca_3(PO_4)_2 + 7H_2O \rightarrow Ca_8(HPO_4)_2(PO_4)_4{\cdot}5H_2O + Ca(OH)_2$. However, this equation implies an increase in the solution pH, which is connected to the direct uptake of PO_4^{3-} into the OCP phase and an equivalent release of soluble calcium hydroxide

($Ca(OH)_2$). As it was seen by the XRD patterns, DCPD was formed as an intermediary phase during the hydrolysis, which was not shown in this equation, hence the general chemical reaction is inadequate. With the observed changes in the pH (Fig. 5) and with the indispensable help of Professor Christian Rey from the University of Toulouse, the progression from LT-α-TCP to OCP was broken down into several distinct steps, as outlined below.

1. Dissolution step.

Before the addition of LT-α-TCP, the orthophosphoric acid solution pH was 2.80 ± 0.15, and once the precursor was added, the solution pH rapidly increased and stabilized at 6.69 ± 0.08 after 1 h. This initial event aligned with the fast dissolution of LT-α-TCP and could be represented by the equation $Ca_3(PO_4)_2 + 3H_2O \rightarrow 3Ca^{2+} + H_2PO_4^- + HPO_4^{2-} + 3OH^-$ (which corresponds to the 6.69 pH). Moreover, it ensures a release of OH^-, which sets the reaction medium at an almost neutral pH related to the buffering zone of orthophosphate anions. A distinct change in the phases was evident when the progression was observed via SEM. The presence of LT-α-TCP, presented with thin thread-like crystals, was seen; however, due to the ongoing dissolution process, small needle- or plate-like crystals started to appear within the LT-α-TCP agglomerates (Fig. 6, 1 h).

2. Precipitation step.

Given the solubility characteristics of LT-α-TCP and the initial acidic dissolution that shifted the solution pH towards an alkaline environment, the resulting solution is supersaturated regarding OCP, DCPD, and even HAp. Nevertheless, HAp had a smaller incline to form than the other two phases due to their better ability to nucleate and grow (higher crystallization rates) [53,54].

3. Growth step of DCPD and OCP phases.

Due to the preferential crystal growth rate of DCPD, LT-α-TCP to DCPD conversion was faster than that of LT-α-TCP to OCP. The following equation can be used as a representation of the process: $Ca_3(PO_4)_2 + 3H_2O \rightarrow 3Ca^{2+} + H_2PO_4^- + HPO_4^{2-} + 3OH^-$, raising the pH up to 7.32 ± 0.07 (Fig. 5). XRD patterns follow the chemical equation, and at the highest pH value (48 h, OCP3 synthesis), the (020) maximum, 11.7 2θ degrees, intensifies markedly compared to any other diffraction peak, pointing at the presence of DCPD (Fig. 5). Hydrolysis, as a continuous process, resulted in a mixture of OCP and DCPD in the system. With making a parallel to SEM findings, it could be corroborated that at 24 h, 30 h, and 48 h time points, when the amount of DCPD increased, a gradual change from thread-like particles to larger and thicker plate-like particles was observed (Fig. 6, 24 h, 30 h, 48 h). Larger and considerably more massive plates were ascribed to DCPD (Fig. 6, 30 h, yellow arrow) and smaller, thinner plate-like crystals to OCP (Fig. 6, 30 h, yellow circle). However, this is difficult to differentiate due to the high morphological similarity of the two phases.

4. DCPD to OCP conversion step.

By complete dissolution of LT-α-TCP, DCPD became the most soluble phase of the system and the precursor for the transformation into OCP, showed in the final equation:

$8\ CaHPO_4 \cdot 2H_2O \rightarrow Ca_8(PO_4)_4(HPO_4)2 \cdot 5H_2O + 2H_3PO_4 + 11H_2O.$

This reaction leads to the release of protons into the solution, which, together with the buffering properties of the present phosphate medium, results in the final pH of 6.44 ± 0.05. At the end

of the synthesis, OCP's plate-like morphology, with noticed fragmentation of the larger particles and the presence of the spherical aggregates could be detected (Fig. 6, 180 h).

By using the Rietveld refinement and SEM [52], the progression of the OCP and intermediary phase formation has also been quantified and, together with their morphology, displayed in Fig. 6. The phases evolved with time from 100 % of LT-α-TCP (in the first hour) to ~ 37 % of DCPD and ~ 63 % of OCP (at 27 h) and ended with ~ 100 % of OCP.

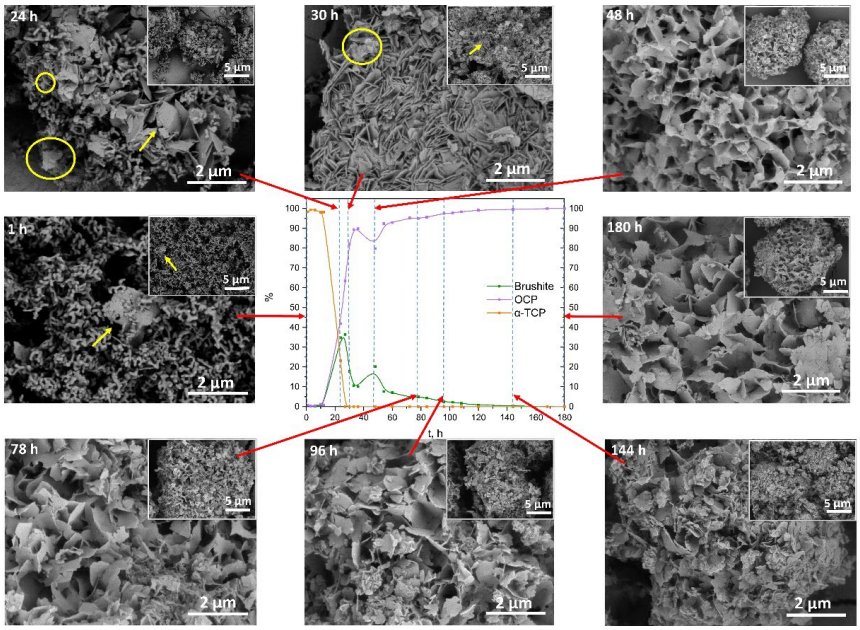

Fig. 6. SEM micrographs of OCP formation (scale bar 5 µm and 2 µm) connected (red arrow) to the according point (dashed line) in the phase content diagram constructed on the XRD quantitative data. The yellow arrow directs to potential DCPD particles, while the yellow circle marks the potential OCP plates [45].

To check if the scaled-up technology affects the cytocompatibility of OCP, the intermediate products and final products of the OCP3 synthesis were subjected to direct contact with human bone mesenchymal stem cells (hBMSC) and the results were compared with OCP1 and OCP2 (Fig. 7 A). The 'Control' represented cells cultivated on polystyrene without CaP powder samples. The results yielded > 80 % of cell metabolic activity. This also indicated that if the technology were upgraded even more in the future, the trace amounts of transient phases and the final phase would be safe for the cells of the bone microenvironment. Visual analysis coupled with immunofluorescent staining, intended to show the cell morphology, indicated a possible CaP particle internalization within the cells when hBMSCs were subjected to direct contact with the powders (Fig. 7 B).

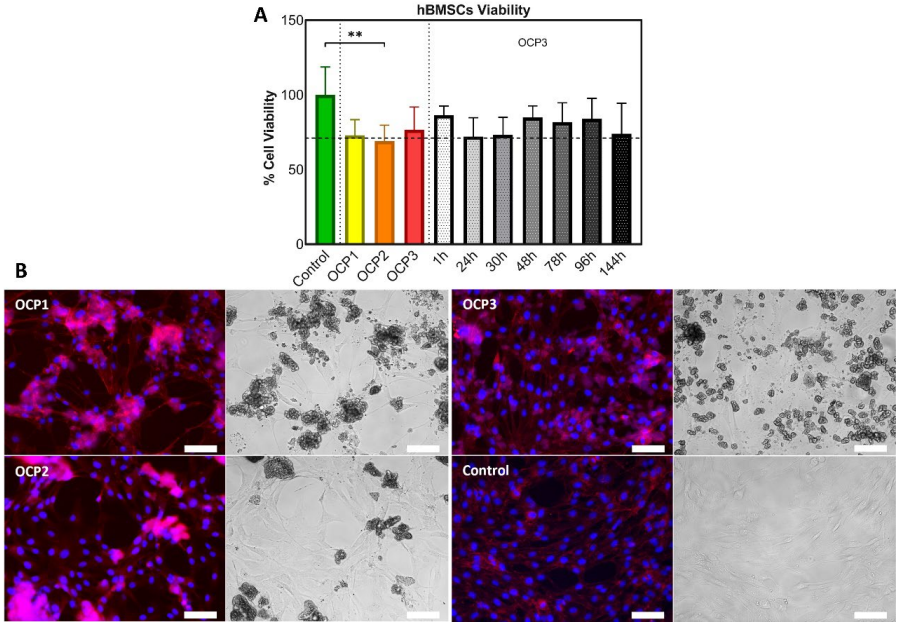

Fig. 7. A – *In vitro* cell viability of OCP1, OCP2, OCP3 and intermediary phases during OCP3 synthesis. Based on one-way ANOVA with Tukey's correction, significant differences between groups of samples were indicated with asterisks (** for $p \leq 0.01$). B – hBMSCs morphology on the third day of cultivation in direct contact with final OCP samples (OCP1, OCP2, OCP3) in the concentration of 0.5 mg/mL. Control represented cells on polystyrene. Immunofluorescent (left columns) and bright-field (right columns) microscopy. Image bar scale: 125 µm.

In silico **modelling of the synthesis progression from LT-α-TCP to OCP**

Conducting comprehensive laboratory experiments is essential for producing and evaluating engineered biomaterials. This includes synthesizing and characterizing their properties and examining the biocompatibility between the surface's physicochemical properties and the adjacent biological microenvironment. However, the chemistry of CaP is exceptionally diverse, allowing for the potential formation of numerous phases depending on specific experimental conditions. Furthermore, the actual experiment conditions may deviate slightly from the intended ones, and this could be attributed to factors such as experimental errors or approximations. To advance towards the new era of artificial intelligence (AI) and to strengthen the collaboration with the University of Eastern Piedmont, together with Dr. M. Nascimben et al. [55] we have developed an automated analysis sequence designed to create a decision support system for monitoring the synthesis progression from LT-α-TCP to OCP.

The goal was to combine the computational protocols capable of determining the synthesis stage (or potential end of it) and the data retrieved from the XRD and FTIR patterns from OCP3 synthesis (10 g yield, 180 h). The analysis sequence contained machine learning (ML)

techniques for feature ranking, spatial filtering, and dimensionality reduction, which were needed in order to tune the automatic recognition of the synthesis stages (Fig. 8).

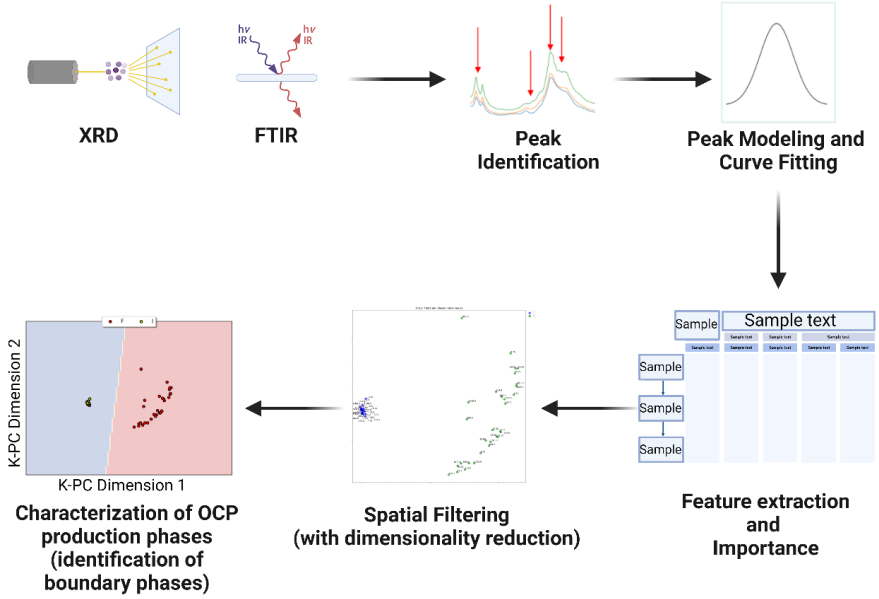

Fig. 8. Schematic process of establishing the machine learning technique for determining the stage of OCP production based on XRD and FTIR spectra [55].

The synthesis progression was monitored with XRD and FTIR (see the previous chapter), and the first two time points (i.e., 1 h and 24 h), as well as the last two time points (144 h and 180 h), were chosen as representative for the initial and final stage of the synthesis, respectively. The analysis pipeline then subjected this data to a preprocessing technique used in ML, called spatial filtering, which enhanced the separation between different classes or patterns from XRD/FTIR. This subset was then employed to recognize OCP production phases.

The combination of expertise in synthesizing and characterizing OCP and a newly developed algorithm capable of identifying at which stage the production of OCP is has brought a promising foundation for a decision support system explicitly tailored for OCP synthesis monitoring. Integration of XRD/FTIR data sets and AI would enable researchers to construct a more robust and informative feature set for training the machine-learning model, which would ultimately lead to a more balanced and accurate model with reduced bias and variance.

Application potential of OCP

As one of the important components of bone tissue inorganic phase, OCP has extensive application possibilities in bone tissue engineering. Its significance stems from the ability to release crucial calcium and phosphate ions in the human body, essential for regulating the new bone deposition. Up until now, OCP has been functionalized as a bone cement [34], a composite scaffold with different polymers (alginate, gelatin, collagen, PEGT, etc.) [35–37], as a coating on titanium or titanium alloy implants [29,38] and as a drug/ion delivery vehicle [23], but clinical applications of the OCP-based biomaterials currently remain at the starting point.

To test the OCP biological potential and to bridge the gap towards clinical application, in the second part of the PhD research, OCP was utilized in the development of two composite biomaterials for the biomedical field. Firstly, OCP was doped with doxorubicin hydrochloride to create an effective drug delivery system for bone cancer treatment. Secondly, OCP was combined with alginate in a composite coating on 3D-printed titanium alloys to test whether it could improve their corrosion resistance.

Octacalcium phosphate and doxorubicin hydrochloride: novel drug delivery system for cancer treatment

Doxorubicin hydrochloride (DOX, doxorubicin), derived from *Streptomyces peucetius var. caesius*, water-soluble and photosensitive, is one of the widely used representatives of anti-cancer drugs [56]. Even though DOX is an effective anti-neoplastic agent it causes multiple systemic toxicities, extending from nausea and hematopoietic suppression to an increased risk of doxorubicin-induced cardiomyopathy [57,58]. Moreover, only a small fraction of any systemically given dose reaches the surgical site. Thus, the use of local anticancer delivery systems could be a solution to achieve high drug levels at the cancer site. Exploring the inherent pathways of programmed cell death (PCD) such as apoptosis, necrosis, or ferroptosis is crucial for tissue engineering (to mimic natural tissue development), drug development (drugs exert their effects by inducing or inhibiting PCD), therapeutic strategies and normal cellular development (eliminating unwanted or damaged cells) [59,60]. Given that the malfunction of intracellular pathways is also a potential trigger for cancer initiation in the human body, comprehending whether PCD is attributed to apoptosis (the death of cells that occurs as a normal and controlled part of development) or ferroptosis (the death of cells that occurs due to genetic changes in iron homeostasis) can contribute to the development of innovative drug delivery systems for future cancer treatments.

Execution of OCP synthesis at room temperature has demonstrated the potential for *in situ* drug loading. The significance lies in the hypothesis that achieving drug loading during the initial stages of OCP formation can result in an exceptionally high drug encapsulation capacity [41]. Given that the stages of LT-α-TCP transformation to OCP involve the release of OH^- and HPO_4^{2-}, they also play a role in the formation of the hydrated layer in the OCP. This, in turn, reinforced the idea that incorporating DOX during the *in situ* OCP synthesis could potentially result in drug loading within the hydrated layer. At the same time, a high specific surface area

of OCP that was achieved and its plate-like particle morphology, potentially make OCP more effective and more favorable in regard to cell responses. Thus, to develop a novel DDS, the emphasis was placed on three steps:

1) **materials' physicochemical property profile** once it was functionalized with DOX in a large concentration range (from 1 wt% to 20 wt% of theoretical LT-α-TCP content);

2) ***in vitro* release kinetics of doxorubicin** during the period of six weeks; and

3) **assessment of the cytocompatibility and the mechanism of PCD**.

A schematic representation of the development of doxorubicin-loaded octacalcium phosphate (DOX-OCP) as a drug delivery system is shown in Fig. 9 [61].

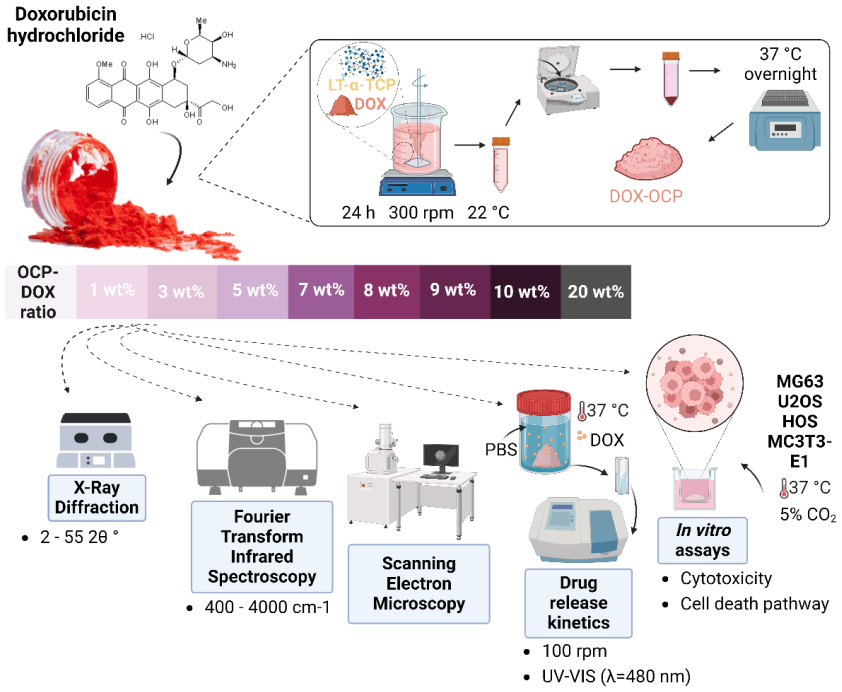

Fig. 9. Schematic representation of the development and characterization approach of doxorubicin-loaded octacalcium phosphate.

To test the maximum amount of DOX incorporation while still preserving the OCP phase 1 wt%, 3 wt%, 5 wt%, 7 wt%, 8 wt%, 9 wt%, 10 wt%, and 20 wt% DOX (of initial LT-α-TCP amount; 1DOX-OCP, 3DOX-OCP, 5DOX-OCP, 7DOX-OCP, 8DOX-OCP, 9DOX-OCP, 10DOX-OCP, 20DOX-CaP) were added to the OCP synthesis medium, and the synthesis lasted for 24 h. By means of XRD analysis, the representative OCP diffraction maxima (low angle (100) maximum, at 2θ = 4.7 degrees and a doublet (200) and (010) at 9.4 degrees and 9.7 degrees) have been detected in the synthesis products where up to 10 wt % of DOX was added (Fig. 10 A and B). If compared with pure OCP, DOX-OCP diffractograms exhibited a slight shift of the maxima 4.7 2θ degrees and 26.1 2θ degrees towards the lower 2θ degrees and a change in intensity. This indicates the lattice expansion in the DOX-OCP system, which

suggests that the drug was incorporated into the crystal structure of OCP. Moreover, the stabilization of the OCP structure depends on the amount of DOX used for the OCP-DOX synthesis. When the quantity of added DOX was above 10 wt%, it hindered the c-axis growth in the OCP structure and destabilized the overall transformation process from LT-α-TCP to OCP. XRD patterns of the tested materials showed that the prominent maxima for LT-α-TCP still persisted at 12.1 and 30.7 2θ degrees, with double maxima at approximately 22.8 and 34 2θ degrees (Fig. 10 A and B) [61]. This means that the drug was being adsorbed onto the LT-α-TCP phase, and the inability of LT-α-TCP to dissolve led to the formation of LT-α-TCP-DOX DDS and not DOX-OCP, which was the set goal.

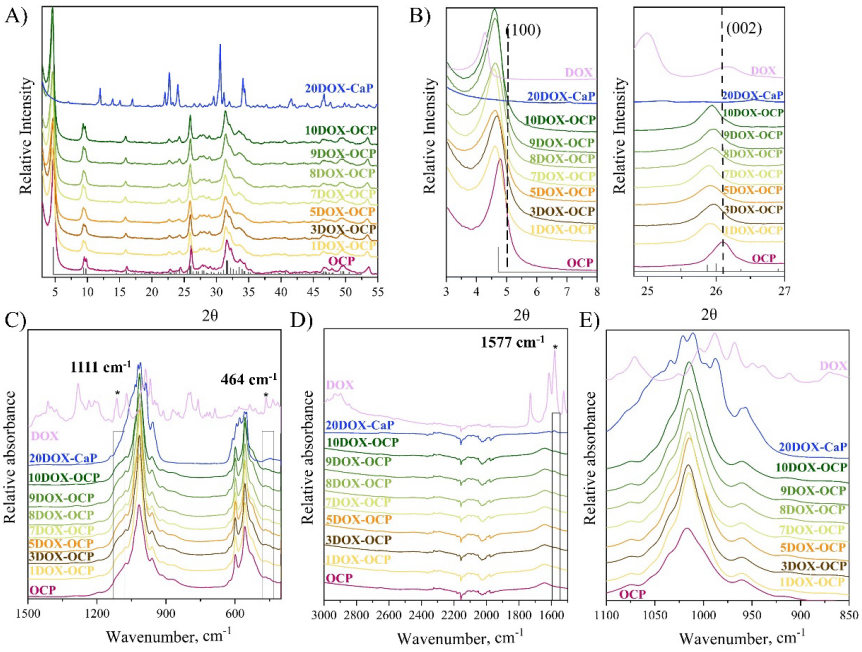

Fig. 10. Physicochemical property profile of DOX-OCP: A – XRD patterns, where ICDD entry #026-1056 corresponds to OCP triclinic phase; B – XRD patterns of OCP and DOX-OCPs. Maxima at 4.7 2θ degrees and 26.1 2θ degrees correspond to (100) and (002) planes, respectively; C, D – FTIR spectra of DOX-OCP. The star and the combining brackets mark the bands that have changed due to DOX incorporation.

Based on FTIR analysis, all of the products (aside 20DOX-CaP) have typical absorbance bands of the OCP phase (Fig. 10 C and D): 1077 cm^{-1}, 1296 cm^{-1}, and 1120 cm^{-1} from the PO_4^{3-} ν_3 stretching mode, and 524, 560, 601, and 627 cm^{-1} from PO_4^{3-} ν_4 domain. Furthermore, P-OH stretching at 917 cm^{-1} and 861 cm^{-1}, associated with the HPO_4^{2-} ion, has been seen. To a certain degree, the influence of strong DOX absorbance bands can also be seen in DOX-OCPs. The increasing intensity of the band in the 1570 cm^{-1} region (Fig. 10 D) signifies an antisymmetric COO^- stretch that could form a strong DOX absorbance band in that position. Moreover, DOX's prominent peak at ~ 1111 cm^{-1} led to a widening of the PO_4^{3-} ν_3 stretching

domain compared to the same region in pure OCP. Consequently, a slight shoulder band can be discerned in the FT-IR spectra of DOX-OCP systems (Fig. 10 C). Bands at 1193 cm^{-1}, associated with HPO_4(5), showed reduced intensity with the increase in DOX content in DOX-OCP systems, suggesting the beginning of OCP hydrolysis to CDHAp.

After the loading of DOX, OCP's plate-like particles appeared to be more overlapping and entwining with the increase of DOX amount in the samples, consequently directing them to form agglomerates in the size of 1–20 μm (Fig. 11 A–G). As it was found previously both in XRD and FTIR data analysis, the highest wt% of the theoretically applied amount of DOX (20 wt%) led to the inhibition of the OCP phase and preservation of elongated grain-like particles typical for α-TCP (Fig. 11 H) [61].

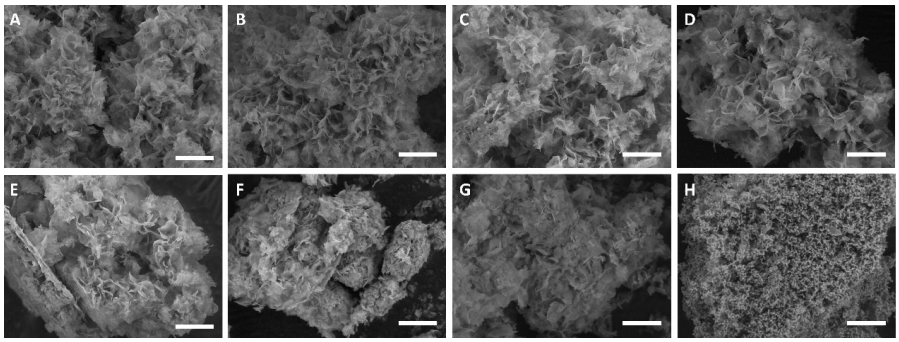

Fig. 11. SEM micrographs of DOX-OCP (1–10 wt%) and DOX-CaP (20 wt%): a – 1 wt%, b – 3 wt%, c – 5 wt%, d – 7 wt%, e – 8 wt%, f – 9 wt%, g – 10 wt%, and h – 20 wt%; scale bar is 5 μm.

For the theoretical DOX loading content of 1 wt%, 5 wt%, and 10 wt% (content), the amount of incorporated DOX was 0.093 ± 0.01 wt% with the loading efficiency of 9.6 ± 1.9 %, 1.54 ± 0.1 wt% with the loading efficiency of 20.85 ± 1.29 % and 2.02 ± 0.06 wt% with the loading efficiency of 21.8 ± 0.73 %, respectively (Fig. 12 A). Nonetheless, when 20 wt% of DOX was used in the OCP synthesis, which did not result in the OCP phase formation, the highest DOX incorporation of 2.66 ± 0.24 wt% was observed. However, the loading efficiency was relatively low – 15.99 ± 1.36 %. This simultaneous action of drug adsorption on the surface may have hindered the formation of OCP while exhibiting a higher detected drug content [61].

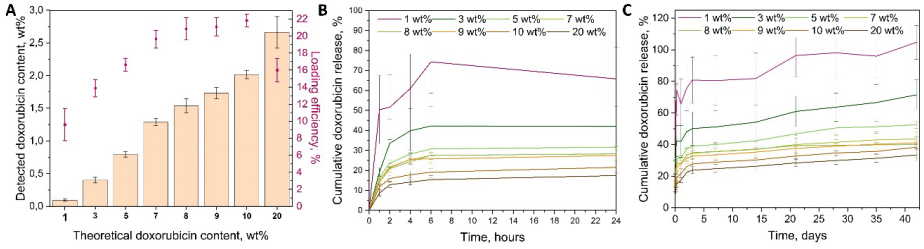

Fig. 12. A – Total DOX content and DOX loading efficiency in DOX loaded samples; B – DOX initial burst release in the first 24 h (%); and C – total DOX release during six weeks (%).

When analyzing DOX release from the developed DOX-OCP delivery systems, it was observed that within the first 24 hours, an early burst release of DOX occurred, ranging from approximately 17 % to 75 % (Fig. 12 B) from the total amount of DOX in the DDS. Subsequently, a sustained and consistent release was monitored for up to six weeks (Fig. 12 C). The initial burst release of doxorubicin molecules from the surface of OCP may be attributed to the physical adsorption of the drug, driven by electrostatic forces or hydrogen bonding. This occurs between the positively charged DOX molecules and the negatively charged OCP. In contrast, the continued release of DOX thereafter may be elucidated by a robust chemical interaction (Ca–O), which hinders the drug's escape from the DOX-OCP drug delivery system [61]. Furthermore, it was found that the cumulative release percentage plateau was inversely proportional to the theoretical doxorubicin content. For instance, in the case of 5DOX-OCP, 23.6 ± 1.6 % (28.00 ± 3.68 μg) was released after two hours, 38.9 ± 1.3 % (46.3 ± 4.2 μg) after 72 hours, and 52.5 ± 2.3 % (62.3 ± 5.8 μg) after 42 days. Meanwhile, the 10DOX-OCP reached 15.9 ± 1.3 % after two hours, 27.7 ± 1.7 % after 72 hours, and 38.3 ± 2.0 % after 42 days. It was observed that the lower the amount of incorporated doxorubicin, the higher the drug release rate. This observation may be attributed to the phase transformation of OCP to calcium-deficient hydroxyapatite [62,63], while lower drug amounts may lead to a faster transformation, consequently resulting in a quicker release. It was also determined that for all DOX-OCPs, the active substance was released gradually from the DDS, and the release profile followed the Freundlich isotherm [63].

***In vitro* assays**

The influence of DOX on MG63 (cancer cells) and MC3T3-E1 (normal cells) cells was studied to compare the cell response to the DOX-OCP drug delivery system. The inclusion of both cell lines allows for a comprehensive analysis of the system's effectiveness in bone cancer treatment and post-tumor excision treatments, offering insights into its potential to reduce metastases. The impact of DOX release on MG63 and MC3T3-E1 cell viability was assessed by exposing cells to OCP and DOX-OCPs (Fig. 13 A). Obtained results revealed that the culture medium treated with 1DOX-OCP, 5DOX-OCP, and 10DOX-OCP suppressed MG63 cells over the course of 7 days (54.1 %, 12.4 %, and 5.7 % of cell viability, respectively). On the other hand, between day 3 and day 7 of MC3T3-E1 cell cultivation, pure OCP, 1DOX-OCP, and

5DOX-OCP demonstrated a stimulatory effect, leading to an increase in cell viability (from 58.5 % to 93.4 % for 1DOX-OCP and from 36.9 % to 67.4 % for 5DOX-OCP). The increase in viability could be due to the cell's slow adjustment to stress caused by the changes or due to the presence of elevated Ca^{2+} ion concentration in the cell medium released from OCP that activated the extracellular calcium-sensing receptors and enhanced the proliferation of the cells [64,65]. The inhibitory effect of 10DOX-OCP on cell viability was notably greater than that of 5DOX-OCP and 1DOX-OCP, providing further evidence of its pronounced inhibitory effect on MG63 cells (Fig. 13 A).

As the preliminary viability tests showed that the DOX-OCP system is lethal to MG63 cells in all concentrations, the lowest incorporated DOX was chosen for further analysis. To assess PCD in osteosarcoma cells (OS), more variety in used cell lines was needed as OS have high genetic heterogeneity. Due to them having different phenotypes, they can express different differentiation capacities and tumour formation capacities and as a result, they can have diverse responses to certain treatments. Hence, 1DOX-OCP was retested with U2OS, MG63, and HOS cell lines. All of the three chosen cell lines are human cell lines commonly used in research; however, they have genetic and phenotype differences, which are preferred for pre-clinical assessments. Similar to the previous cytocompatibility assessments, the outcomes showed a noteworthy reduction in the viability of all examined osteosarcoma cells when exposed to 1DOX-OCP (MG63 – 0.32 ± 0.2 %, HOS – 0.17 ± 0.02 %, and U2OS – 0.25 ± 0.02 % of cell viability) (Fig. 13 B). The variances in cell viability between 1DOX-OCP and DOX may stem from the immediate accessibility of the drug at its final concentration in the positive control group (DOX), whereas doxorubicin from 1 wt % of DOX-OCP was released gradually over time, aligning with the findings of the *in vitro* drug release study (Fig. 12 B and C). To see whether the sensitivity of OS cells will increase towards the ferroptosis, DOX-OCP was combined with the ferroptosis inhibitor Ferrostatin-1 (Fer-1) [66]. The results showed no significant difference (Fig. 13 C) in OS cell survival in the presence of 1DOX-OCP+Fer-1 compared to 1DOX-OCP alone (Fig. 13 C). This pointed out that ferroptosis is not involved in DOX-OCP-induced cell death in OS cells. As ferroptosis was excluded, the next step was to check apoptosis by testing the levels of cleaved poly (ADP-ribose) polymerase (PARP) [67,68], considered as a guarantee of apoptosis by western blotting analysis. Results showed increased expression of cleaved PARP in HOS and MG-63 cells exposed to 1DOX-OCP, confirming the induction of apoptotic cell death (Fig. 13 D) [61]. The *in vitro* assays were done in collaboration with Dr. E. Panczyszyn from the University of Eastern Piedmont in Italy and with Dr. O. Demir from the Riga Technical University.

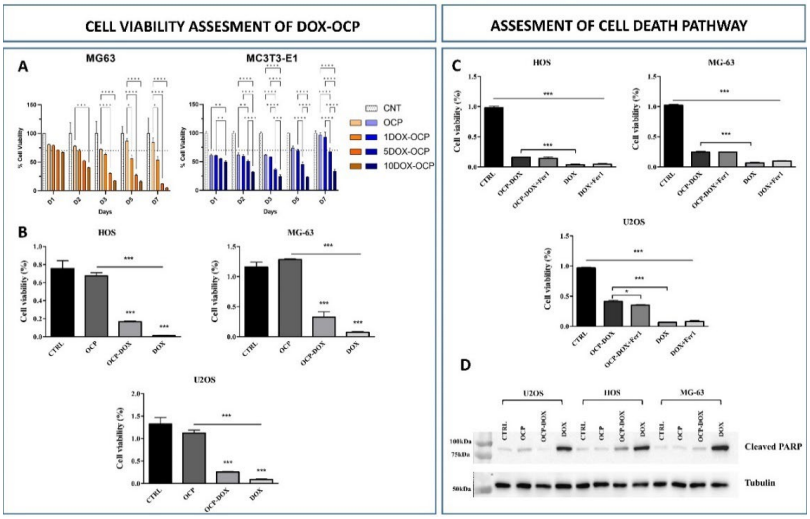

Fig. 13. Cell viability studies of DOX-OCP. A – Cell viability assay of MG63 cells and MC3T3-E1 cells with OCP, 1DOX-OCP, 5DOX-OCP, and 10DOX-OCP; B – Sensitivity of OS cells to 1DOX-OCP, OCP, and DOX; C – cell viability of U2OS, HOS, and MG63 cells in combination with 10 μM of Fer1 (1DOX-OCP+Fer-1, DOX+Fer-1); D – Protein levels of cleaved PARP. Histograms represent mean ± s.d.; $n = 3$; statistically significant differences: * for $p < 0.05$, ** for $p < 0.005$, *** for $p < 0.001$, **** for $p < 0.0001$.

OCP-embedded hydrogel coatings as metallic implant anticorrosion enhancers

Titanium alloys (Ti) are extensively utilized as biomaterials for fabricating dental and orthopedic implants, primarily owing to their exceptional mechanical characteristics and favorable biocompatibility. These alloys exhibit reasonable corrosion resistance under typical physiological conditions (pH ≈ 7), as their surfaces are naturally enveloped with dense protective oxide layers. Nevertheless, in inflammatory conditions that lower the environment pH, interactions with reactive oxygen species, lactic acid, hydroperoxyl radicals, and hypochlorous acid (released by leukocytes into the extracellular environment) affect the corrosion resistance of Ti surfaces. An effective strategy for improving corrosion resistance is surface modification of Ti by hydrogel coatings. To test whether the OCP particles improve the Ti protection even further, a collaboration was formed with Aalto University. Together with Dr. A. Bordbar-Khiabani et al. [38], sodium alginate (Alg) and OCP powder were combined in a composite coating and tested for their electrochemical behavior on Ti alloys. A schematic representation of the experimental setup is shown in Fig. 14.

In brief, aqueous Alg solution (3 wt %) and OCP were combined into a composite having a 70 : 30 wt% inorganic : organic phase ratio (later referred to as Alg/OCP) and further used to cover the surface of 3D-printed titanium substrates. Titanium alloy discs (d = 10 mm) – Ti Gr2 and Ti Gr23 alloy were covered with approximately 10 mg of the coatings (Alg and Alg/OCP) and compared with respect to their performance against corrosion. To test the effects of the

inflammatory conditions, three simulation media with pH 7.4 ± 0.1 (normal – N), pH 5.2 ± 0.1 (inflammatory – I) and pH 3.0 ± 0.2 (severe inflammatory – SI) were made, and immersion tests were performed at 37 ± 0.5 °C in slightly anaerobic conditions.

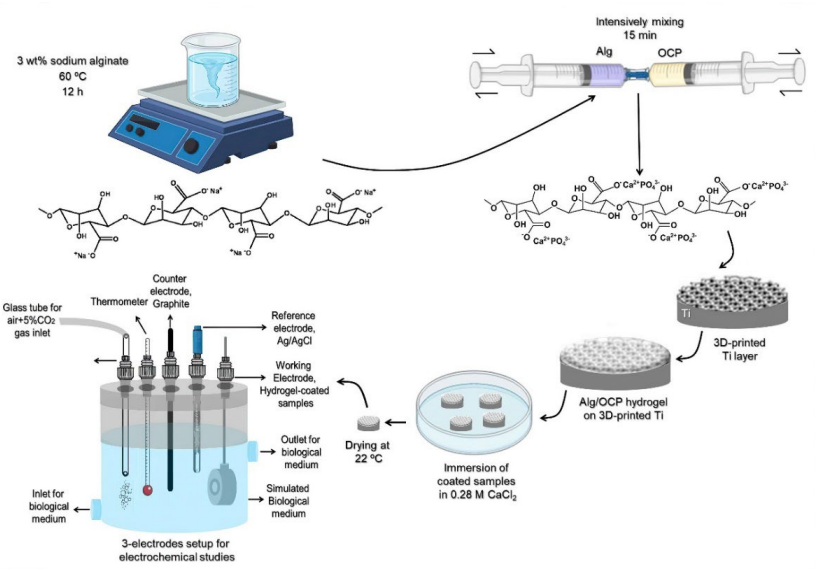

Fig. 14. Schematic representation of the experimental set-up for obtaining and electrochemical characterization of 3D printed Ti alloys with Alg/OCP coating [38].

Physicochemical properties of the coatings were characterized prior to (marked as Alg/OCP) and after one hour-long immersions in the respective media – marked as Alg/OCP N, I, SI (Fig. 15). Characteristic XRD diffraction maxima of OCP were observed, and an amorphous broad halo that was seen in the XRD pattern was specific to sodium-alginate biopolymer (Fig. 15 A). FTIR showed the vibrations of HPO_4^{2-} at 917 cm^{-1}, 875 cm^{-1}, 1007 cm^{-1}, and 1295 cm^{-1} that belong to OCP and a broad band centered at approximately 3500 cm^{-1}, which corresponds to the stretching vibrations of the hydroxyl groups (Fig. 15 B).

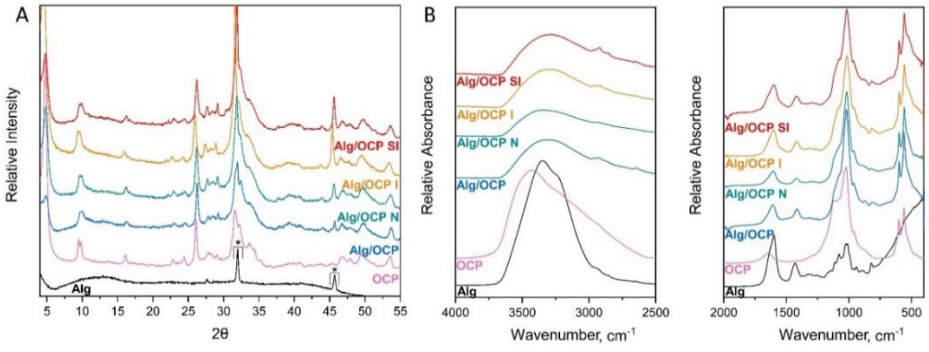

Fig. 15. Physico-chemical characterization of Alg/OCP coating prior to and after the immersion in the respective media (normal – N, inflammatory – I, and severely inflammatory – SI). A – XRD patterns, B – FTIR spectra in different wavenumber regions [38].

Electrochemical impedance spectroscopy (EIS) is usually used to characterize the electrochemical processes, such as the evaluation of the performance of protective coatings on metals against corrosion. The Nyquist plot was used as a frequency response plot and the Bode modulus was used to represent the gain and phase of a system as a function of frequency. The obtained results of EIS and the constant phase element (CPE) [69] (measurement of coating's capacity shown via CPE_{dl} (interface between a substrate and a solution) and Rct (resistance to charge transfer)) were presented and explained in detail within the A. Bordbar-Khiabani et al. study [38].

Shortly, the Nyquist plots for both inflammatory and severely inflammatory conditions illustrated a declining pattern in the capacitive loop diameters, which indicated a reduction in the corrosion resistance [69,70] and the Bode amplitude plot, shown in the low-frequency range of the impedance modulus, also corroborated this trend [38]. The Rct values of samples with Alg/OCP coatings were notably greater (23.09 ± 0.10 k$\Omega \cdot cm^2$ and 25.12 ± 0.39 k$\Omega \cdot cm^2$ for TiGr2 and TiGr23, respectively) than those of the bare 3D-printed Ti samples (17.63 ± 0.33 k$\Omega \cdot cm^2$ and 20.66 ± 0.73 k$\Omega \cdot cm^2$ for TiGr2 and TiGr23, respectively). This suggests that the Alg/OCP coating effectively forms a robust barrier, impeding the penetration of corrosive ions into the substrate. Additionally, the presence of OCP further enhanced the resistance (Rc) of Alg hydrogel (e.g., 12.33 ± 0.83 k$\Omega \cdot cm^2$ Alg and 18.84 ± 0.75 k$\Omega \cdot cm^2$ Alg/OCP for TiGr2), suggesting that OCP particles may fortify the crosslinking degree of the Alg hydrogel coating and enhance the bonding force at the interface between the coating and the substrate in normal conditions. This led to an increase in the coating's density. Consequently, the Alg/OCP-coated samples exhibited higher Rc values than those coated with pure Alg. The reduction in Rc values observed in coated samples under inflammatory and severe inflammatory conditions (e.g., I: 7.15 ± 0.91 k$\Omega \cdot cm^2$ Alg/OCP and SI: 3.01 ± 0.53 k$\Omega \cdot cm^2$ Alg/OCP for TiGr2) can be attributed to the hydrogels becoming less stable due to their dissolution by hydrochloric acid and hydrogen peroxide [38,69].

CONCLUSIONS

1. Tenfold and hundredfold scale-up of the hydrolysis (from LT-α-TCP) yielded the final 1 g and 10 g of pure OCP; however, the increase of the synthesis yield required the extension of the synthesis duration from 72 h (1 g) to 180 h (10 g).

2. LT-α-TCP transformation into the OCP phase transpired through brushite as an intermediary phase.

3. During the synthesis of the DOX-OCP drug delivery system, the addition of > 10 wt% of doxorubicin (from the initial LT-α-TCP amount) inhibits OCP phase formation.

4. DOX-OCP alters the proliferation profile of MG63 and MC3T3 cells, which is influenced by both DOX concentrations in the cell medium and the contact time of DOX-OCP/cell environment.

5. Apoptosis was the primary pathway of programmed cell death induced in osteosarcoma cells by the DOX-OCP drug delivery system.

6. OCP particles in the alginate hydrogel matrix increased the electrical charge transfer resistance at the Ti substrate and alginate/OCP coating interface.

REFERENCES

[1] S. Liu, B. Wang, S. Fan, Y. Wang, Y. Zhan, D. Ye, Global burden of musculoskeletal disorders and attributable factors in 204 countries and territories : a secondary analysis of the Global Burden of Disease 2019 study, BMJ Open. 12 (2022). https://doi.org/10.1136/bmjopen-2022-062183.

[2] B.E. Wilson, S. Jacob, M.L. Yap, J. Ferlay, F. Bray, M.B. Barton, Estimates of global chemotherapy demands and corresponding physician workforce requirements for 2018 and 2040: a population-based study, Lancet Oncol. 20 (2019) 769–780. https://doi.org/10.1016/S1470-2045(19)30163-9.

[3] T. Albrektsson, C. Johansson, Osteoinduction, osteoconduction and osseointegration, Eur Spine J. 10 (2001) 96–101.

[4] C. Rey, C. Combes, C. Drouet, M.J. Glimcher, Bone mineral: Update on chemical composition and structure, Osteoporos. Int. 20 (2009) 1013–1021. https://doi.org/10.1007/s00198-009-0860-y.

[5] H. Yuan, H. Fernandes, P. Habibovic, J. De Boer, A.M.C. Barradas, A. De Ruiter, W.R. Walsh, C.A. Van Blitterswijk, J.D. De Bruijn, Osteoinductive ceramics as a synthetic alternative to autologous bone grafting, Proc. Natl. Acad. Sci. U. S. A. 107 (2010) 13614–13619. https://doi.org/10.1073/pnas.1003600107.

[6] T. Ariizumi, H. Kawashima, H. Hatano, T. Yamagishi, N. Oike, Osteoinduction and Osteoconduction with Porous Beta-Tricalcium Phosphate Implanted after Fibular Resection in Humans, J. Biomater. Nanobiotechnol. 10 (2019) 159–173. https://doi.org/10.4236/jbnb.2019.103009.

[7] R.Z. LeGeros, Properties of osteoconductive biomaterials: Calcium phosphates, Clin. Orthop. Relat. Res. (2002) 81–98. https://doi.org/10.1097/00003086-200202000-00009.

[8] W. Habraken, P. Habibovic, M. Epple, M. Bohner, Calcium phosphates in biomedical applications: Materials for the future?, Mater. Today. 19 (2016) 69–87. https://doi.org/10.1016/j.mattod.2015.10.008.

[9] S. V Dorozhkin, M. Epple, Biological and Medical Significance of Calcium Phosphates, Angew. Chem. Int. Ed. 41 (2002) 3130–3146.

[10] T. Wach, M. Kozakiewicz, Fast-Versus Slow-Resorbable Calcium Phosphate Bone Substitute Materials — Texture Analysis after 12 Months of Observation, Materials (Basel). 13 (2020) 3854.

[11] T.J. Brunner, R.N. Grass, M. Bohner, W.J. Stark, Effect of particle size, crystal phase and crystallinity on the reactivity of tricalcium phosphate cements for bone reconstruction, J. Mater. Chem. 17 (2007) 4072–4078. https://doi.org/10.1039/b707171j.

[12] Uskokovic Vuk, T.A. Desai, Phase composition control of calcium phosphate nanoparticles for tunable drug delivery kinetics and treatment of osteomyelitis. I. Preparation and drug release, J. Biomed. Mater. Res. - Part A. 101 A (2013) 1416–1426. https://doi.org/10.1002/jbm.a.34426.

[13] G. Daculsi, R.Z. LeGeros, E. Nery, K. Lynch, B. Kerebel, Transformation of biphasic calcium phosphate ceramics in vivo : Ultrastructural and physicochemical characterization, J. Biomed. Mater. Res. 23 (1989) 883–894.

[14] M.S. Johnsson, G.H. Nancollas, The Role of Brushite and Octacalcium Phosphate in Apatite Formation, Crit. Rev. Oral Biol. Med. 3 (1992) 61–82. https://doi.org/10.1177/10454411920030010601.

[15] J. Vecstaudza, M. Gasik, J. Locs, Amorphous calcium phosphate materials: Formation, structure and thermal behaviour, J. Eur. Ceram. Soc. 39 (2019) 1642–1649. https://doi.org/10.1016/j.jeurceramsoc.2018.11.003.

[16] M. Mosina, J. Locs, Synthesis of amorphous calcium phosphate: A review, Key Eng. Mater. 850 KEM (2020) 199–206. https://doi.org/10.4028/www.scientific.net/KEM.850.199.

[17] N. Temizel, G. Girisken, A.C. Tas, Accelerated transformation of brushite to octacalcium phosphate in new biomineralization media between 36.5 °c and 80 °c, Mater. Sci. Eng. C. 31 (2011) 1136–1143. https://doi.org/10.1016/j.msec.2011.04.009.

[18] A. Dosen, R.F. Giese, Thermal decomposition of brushite, CaHPO4 ·2H2O to monetite CaHPO4 and the formation of an amorphous phase, Am. Mineral. 96 (2011) 368–373. https://doi.org/10.2138/am.2011.3544.

[19] L.C.Chow, E.D. Eanes, Octacalcium phosphate, 2001. https://doi.org/10.1007/springerreference_39293.

[20] C.C. Rey, C. Combes, C. Drouet, Synthesis and physical chemical characterizations of octacalcium phosphate-based biomaterials for hard-tissue regeneration, 2019. https://doi.org/10.1016/B978-0-08-102511-6.00008-X.

[21] O. Suzuki, G. Insley, Octacalcium Phosphate Biomaterials, Woodhead Publishing Series in Biomaterials, 2020.

[22] S. Ban, J. Hasegawa, T. Jinde, Phase Transformation of Octacalcium Phosphate in vivo and in vitro, Dent. Mater. J. 11 (1992) 130–140217. https://doi.org/10.4012/dmj.11.130.

[23] I. Kovrlija, J. Locs, D. Loca, Octacalcium phosphate: Innovative vehicle for the local biologically active substance delivery in bone regeneration, Acta Biomater. 135 (2021) 27–47. https://doi.org/10.1016/j.actbio.2021.08.021.

[24] T. Anada, A. Araseki, S. Matsukawa, T. Yamasaki, S. Kamakura, O. Suzuki, Effect of octacalcium phosphate ionic dissolution products on osteoblastic cell differentiation, Key Eng. Mater. 361-363 I (2008) 31–34. https://doi.org/10.4028/www.scientific.net/kem.361-363.31.

[25] Y. Sai, Y. Shiwaku, T. Anada, K. Tsuchiya, T. Takahashi, O. Suzuki, Capacity of octacalcium phosphate to promote osteoblastic differentiation toward osteocytes in vitro, Acta Biomater. 69 (2018) 362–371. https://doi.org/10.1016/j.actbio.2018.01.026.

[26] Y. Shiwaku, K. Tsuchiya, L. Xiao, O. Suzuki, Effect of calcium phosphate phases affecting the crosstalk between osteoblasts and osteoclasts in vitro, J. Biomed. Mater. Res. - Part A. 107 (2019) 1001–1013. https://doi.org/10.1002/jbm.a.36626.

[27] N. Miyatake, K.N. Kishimoto, T. Anada, H. Imaizumi, E. Itoi, O. Suzuki, Effect of partial hydrolysis of octacalcium phosphate on its osteoconductive characteristics, Biomaterials. 30 (2009) 1005–1014. https://doi.org/10.1016/j.biomaterials.2008.10.058.

[28] F. Barrère, C.M. Van Der Valk, R.A.J. Dalmeijer, G. Meijer, C.A. Van Blitterswijk, K. De Groot, P. Layrolle, Osteogenecity of octacalcium phosphate coatings applied on

porous metal implants, J. Biomed. Mater. Res. - Part A. 66 (2003) 779–788. https://doi.org/10.1002/jbm.a.10454.

[29] P. Habibovic, C.M. Van Der Valk, C.A. Van Blitterswijk, K. De Groot, G. Meijer, Influence of octacalcium phosphate coating on osteoinductive properties of biomaterials, J. Mater. Sci. Mater. Med. 15 (2004) 373–380. https://doi.org/10.1023/B:JMSM.0000021104.42685.9f.

[30] R.Z. LeGeros, Preparation of Octacalcium Phosphate (OCP): A Direct Fast Method, Calcif. Tissue Int. (1985) 194–197.

[31] S. Graham, P.W. Brown, The low temperature formation of octacalcium phosphate, J. Cryst. Growth. 132 (1993) 215–225. https://doi.org/10.1016/0022-0248(93)90265-X.

[32] Christophe Drouet, Apatite formation: why it may not work as planned, and how to conclusively identify apatite compounds., Biomed Res. Int. 2013 (2013) Article ID 490946. http://dx.doi.org/10.1155/2013/490946.

[33] O. Suzuki, Octacalcium phosphate (OCP)-based bone substitute materials, Jpn. Dent. Sci. Rev. 49 (2013) 58–71. https://doi.org/10.1016/j.jdsr.2013.01.001.

[34] O. Demir, A. Pylostomou, D. Loca, Octacalcium phosphate phase forming cements as an injectable bone substitute materials : Preparation and in vitro structural study, Biomater. Adv. J. 157 (2024). https://doi.org/10.1016/j.bioadv.2023.213731.

[35] Y. Tanuma, T. Anada, Y. Honda, T. Kawai, S. Kamakura, S. Echigo, O. Suzuki, Granule size-dependent bone regenerative capacity of octacalcium phosphate in collagen matrix, Tissue Eng. - Part A. 18 (2012) 546–557. https://doi.org/10.1089/ten.tea.2011.0349.

[36] T. Fuji, T. Anada, Y. Honda, Y. Shiwaku, H. Koike, S. Kamakura, K. Sasaki, O. Suzuki, Octacalcium phosphate-precipitated alginate scaffold for bone regeneration, Tissue Eng. - Part A. 15 (2009) 3525–3535. https://doi.org/10.1089/ten.tea.2009.0048.

[37] O. Suzuki, Y. Shiwaku, R. Hamai, Octacalcium phosphate bone substitute materials: Comparison between properties of biomaterials and other calcium phosphate materials, Dent. Mater. J. 39 (2020) 187–199. https://doi.org/10.4012/dmj.2020-001.

[38] A. Bordbar-Khiabani, I. Kovrlija, J. Locs, D. Loca, M. Gasik, Octacalcium Phosphate-Laden Hydrogels on 3D-Printed Titanium Biomaterials Improve Corrosion Resistance in Simulated Biological Media, Int. J. Mol. Sci. 24 (2023). https://doi.org/10.3390/ijms241713135.

[39] M.R. Newman, D.S.W. Benoit, Local and targeted drug delivery for bone regeneration, Curr. Opin. Biotechnol. 40 (2016) 125–132. https://doi.org/10.1016/j.copbio.2016.02.029.

[40] A. Lebugle, A. Rodrigues, P. Bonnevialle, J.J. Voigt, P. Canal, F. Rodriguez, Study of implantable calcium phosphate systems for the slow release of methotrexate, Biomaterials. 23 (2002) 3517–3522.

[41] Q.L. Tang, Y.J. Zhu, J. Wu, F. Chen, S.W. Cao, Calcium phosphate drug nanocarriers with ultrahigh and adjustable drug-loading capacity: One-step synthesis, in situ drug loading and prolonged drug release, Nanomedicine Nanotechnology, Biol. Med. 7 (2011) 428–434. https://doi.org/10.1016/j.nano.2010.12.005.

[42] O. Suzuki, S. Kamakura, T. Katagiri, M. Nakamura, B. Zhao, Y. Honda, R. Kamijo,

Bone formation enhanced by implanted octacalcium phosphate involving conversion into Ca-deficient hydroxyapatite, Biomaterials. 27 (2006) 2671–2681. https://doi.org/10.1016/j.biomaterials.2005.12.004.

[43] Y. Murakami, Y. Honda, T. Anada, H. Shimauchi, O. Suzuki, Comparative study on bone regeneration by synthetic octacalcium phosphate with various granule sizes, Acta Biomater. 6 (2010) 1542–1548. https://doi.org/10.1016/j.actbio.2009.10.023.

[44] Z. Irbe, D. Loca, A. Pura, L. Berzina-Cimdina, Synthesis and properties of α-tricalcium phosphate from amorphous calcium phosphate as component for bone cements, Key Eng. Mater. 721 KEM (2017) 182–186. https://doi.org/10.4028/www.scientific.net/KEM.721.182.

[45] I. Kovrlija, K. Menshikh, O. Marsan, C. Rey, C. Combes, J. Locs, D. Loca, Exploring the Formation Kinetics of Octacalcium Phosphate from Alpha-Tricalcium Phosphate : Synthesis Scale-Up , Determination of Transient Phases , Their Morphology and Biocompatibility, Biomolecules. 13 (2023).

[46] W.E. Brown, M. Mathew, M.S. Tung, Crystal chemistry of octacalcium phosphate, Prog. Cryst. Growth Charact. 4 (1981) 59–87. https://doi.org/10.1016/0146-3535(81)90048-4.

[47] R.A. Terpstra, P. Bennema, Crystal morphology of octacalcium phosphate: Theory and observation, J. Cryst. Growth. 82 (1987) 416–426. https://doi.org/10.1016/0022-0248(87)90333-2.

[48] W.E. Brown, J.R. Lehr, J.P. Smith, A. William Frazier, Crystallography of octacalcium phosphate [5], J. Am. Chem. Soc. 79 (1957) 5318–5319. https://doi.org/10.1021/ja01576a068.

[49] B.O. Fowler, M. Marković, W.E. Brown, Octacalcium Phosphate. 3. Infrared and Raman Vibrational Spectra, Chem. Mater. 5 (1993) 1417–1423. https://doi.org/10.1021/cm00034a009.

[50] M. Robin, S. Von Euw, G. Renaudin, S. Gomes, J.M. Krafft, N. Nassif, T. Azaïs, G. Costentin, Insights into OCP identification and quantification in the context of apatite biomineralization, CrystEngComm. 22 (2020) 2728–2742. https://doi.org/10.1039/c9ce01972c.

[51] N. Döbelin, Validation of XRD phase quantification using semi-synthetic data, Powder Diffr. 35 (2020) 262–275. https://doi.org/10.1017/S0885715620000573.

[52] N. Döbelin, Interlaboratory study on the quantification of calcium phosphate phases by Rietveld refinement, Powder Diffr. 30 (2015) 231–241. https://doi.org/10.1017/S088571561500038X.

[53] J.C. Heughebaert, G.H. Nancollas, Kinetics of crystallization of octacalcium phosphate, J. Phys. Chem. 88 (1984) 2478–2481. https://doi.org/10.1021/j150656a012.

[54] J.P. Barone, G.H. Nancollas, The Seeded Growth of Calcium Phosphates. The Kinetics of Growth of Dicalcium Phosphate Dihydrate on Enamel, Dentin, and Calculus, J. Dent. Res. 57 (1978) 153–161. https://doi.org/10.1177/00220345780570010901.

[55] M. Nascimben, I. Kovrlija, J. Locs, D. Loca, L. Rimondini, Fusion and classification algorithm of octacalcium phosphate production based on XRD and FTIR data, Sci. Rep. (2024) 1–11. https://doi.org/10.1038/s41598-024-51795-0.

[56] S. Sritharan, N. Sivalingam, A comprehensive review on time-tested anticancer drug doxorubicin, Life Sci. 278 (2021) 119527. https://doi.org/10.1016/j.lfs.2021.119527.

[57] S.Y. van der Zanden, X. Qiao, J. Neefjes, New insights into the activities and toxicities of the old anticancer drug doxorubicin, FEBS J. 288 (2021) 6095–6111. https://doi.org/10.1111/febs.15583.

[58] R.D. Olson, P.S. Mushlin, Doxorubicin cardiotoxicity: analysis of prevailing hypotheses, FASEB J. 4 (1990).

[59] X. Liu, S. Du, S. Wang, K. Ye, Ferroptosis in osteosarcoma: A promising future, Front. Oncol. 12 (2022) 1–9. https://doi.org/10.3389/fonc.2022.1031779.

[60] C.M. Pfeffer, A.T.K. Singh, Apoptosis: A target for anticancer therapy, Int. J. Mol. Sci. 19 (2018). https://doi.org/10.3390/ijms19020448.

[61] I. Kovrlija, E. Pańczyszyn, O. Demir, M. Laizane, M. Corazzari, J. Locs, D. Loca, Doxorubicin loaded octacalcium phosphate particles as controlled release drug delivery systems: Physico-chemical characterization, in vitro drug release and evaluation of cell death pathway, Int. J. Pharm. 653 (2024) 1–14. https://doi.org/10.1016/j.ijpharm.2024.123932.

[62] N. Ito, M. Kamitakahara, K. Ioku, Preparation and evaluation of spherical porous granules of octacalcium phosphate/hydroxyapatite as drug carriers in bone cancer treatment, Mater. Lett. 120 (2014) 94–96. https://doi.org/10.1016/j.matlet.2014.01.040.

[63] M. Parent, H. Baradari, E. Champion, C. Damia, M. Viana-trecant, Design of calcium phosphate ceramics for drug delivery applications in bone diseases : A review of the parameters affecting the loading and release of the therapeutic substance, J. Control. Release. 252 (2017) 1–17. https://doi.org/10.1016/j.jconrel.2017.02.012.

[64] M. Akutsu, Y. Kano, S. Tsunoda, K. Suzuki, Y. Yazawa, Y. Miura, Schedule-dependent interaction between paclitaxel and doxorubicin in human cancer cell lines in vitro, Eur. J. Cancer. 31 (1995) 2341–2346. https://doi.org/10.1016/0959-8049(95)00448-3.

[65] J. Wang, J. de Boer, K. de Groot, Proliferation and differentiation of osteoblast-like MC3T3-E1 cells on biomimetically and electrolytically deposited calcium phosphate coatings., J. Biomed. Mater. Res. A. 90 (2009) 664–670. https://doi.org/10.1002/jbm.a.32128.

[66] G. Miotto, M. Rossetto, M.L. Di Paolo, L. Orian, R. Venerando, A. Roveri, A.M. Vučković, V. Bosello Travain, M. Zaccarin, L. Zennaro, M. Maiorino, S. Toppo, F. Ursini, G. Cozza, Insight into the mechanism of ferroptosis inhibition by ferrostatin-1, Redox Biol. 28 (2020) 101328. https://doi.org/10.1016/j.redox.2019.101328.

[67] S. Wang, E.A. Konorev, S. Kotamraju, J. Joseph, S. Kalivendi, B. Kalyanaraman, Doxorubicin induces apoptosis in normal and tumor cells via distinctly different mechanisms: Intermediacy of H2O2- and p53-dependent pathways, J. Biol. Chem. 279 (2004) 25535–25543. https://doi.org/10.1074/jbc.M400944200.

[68] G.V. Chaitanya, J.S. Alexander, P.P. Babu, PARP-1 cleavage fragments: Signatures of cell-death proteases in neurodegeneration, Cell Commun. Signal. 8 (2010) 1–11. https://doi.org/10.1186/1478-811X-8-31.

[69] N. Yoshimoto, I. Wahyudhin, A. Yabuki, Colloids and Surfaces A : Physicochemical and Engineering Aspects Self-healing polymer coating with efficient delivery for

alginates and calcium nitrite to provide corrosion protection for carbon steel, Colloids Surfaces A Physicochem. Eng. Asp. 662 (2023) 130970. https://doi.org/10.1016/j.colsurfa.2023.130970.

[70] A. Bordbar-khiabani, M. Gasik, Electrochemical behavior of additively manufactured patterned titanium alloys under simulated normal , inflammatory , and severe inflammatory conditions, J. Mater. Res. Technol. 26 (2023) 356–370. https://doi.org/10.1016/j.jmrt.2023.07.113.

Ilijana Kovrlija was born in 1994 in Prijedor, Bosnia and Herzegovina. She obtained her Bachelor's degree in Biochemical Engineering and Biotechnology in 2017 and her Master's degree in the same field in 2018, both from the University of Belgrade. In 2020, Ilijana joined the Institute of Biomaterials and Bioengineering at Riga Technical University (RTU) as a PhD candidate within the Marie Skłodowska-Curie ITN programme – PREMUROSA, working on the Doctoral Thesis under the supervision of Professor Dagnija Loča and Professor Jānis Ločs. She is currently a scientific assistant at the RTU Institute of Biomaterials and Bioengineering. During her doctoral studies, Ilijana completed four scientific secondments at *CAAD* – University of Eastern Piedmont (Novara, Italy), *CIRIMAT* – University of Toulouse (Toulouse, France), and AALTO University (Helsinki, Finland). Her research interests include biomaterial synthesis, processing and characterization, as well as the development of drug delivery systems.